

# Microplasmas for Advanced Materials and Devices

Wei-Hung Chiang, Davide Mariotti, R. Mohan Sankaran, J. Gary Eden,  
and Kostya (Ken) Ostrikov\*

Microplasmas are low-temperature plasmas that feature microscale dimensions and a unique high-energy-density and a nonequilibrium reactive environment, which makes them promising for the fabrication of advanced nanomaterials and devices for diverse applications. Here, recent microplasma applications are examined, spanning from high-throughput, printing-technology-compatible synthesis of nanocrystalline particles of common materials types, to water purification and optoelectronic devices. Microplasmas combined with gaseous and/or liquid media at low temperatures and atmospheric pressure open new ways to form advanced functional materials and devices. Specific examples include gas-phase, substrate-free, plasma-liquid, and surface-supported synthesis of metallic, semiconducting, metal oxide, and carbon-based nanomaterials. Representative applications of microplasmas of particular importance to materials science and technology include light sources for multipurpose, efficient VUV/UV light sources for photochemical materials processing and spectroscopic materials analysis, surface disinfection, water purification, active electromagnetic devices based on artificial microplasma optical materials, and other devices and systems including the plasma transistor. The current limitations and future opportunities for microplasma applications in materials related fields are highlighted.

## 1. Introduction

Low-temperature plasmas have been used for decades as a reactive environment for advanced materials fabrication and active media in functional devices. Common examples of materials and processes that benefit from plasmas include silicon deposition, photoresist etching, surface cleaning for the microelectronic, automotive, and several other industries that rely on sophisticated materials processing. Low-pressure, low-temperature plasmas have been highly successful in the manufacturing of microelectronic components. Plasma processes are used in the key technological steps involving thin film etching and deposition and help drive miniaturization to sustain technology development according to Moore's Law and increasing the computing power required for communications, security, traffic control, healthcare as well as for other applications such as solar energy.

With the recent advances in nanotechnology, device miniaturization, and other areas, it has become increasingly

important to explore alternative materials synthesis and processing environments that rely on concentrating electromagnetic energy and exciting gas molecules in small volumes. This ability is required, e.g., in generating reactive species in the gas or vapor phases that subsequently emit radiation or produce a desired material by heterogeneous chemistry at a surface. In this way, advanced materials with nanoscale features can be synthesized and unique combinations of reactive species and radiation under nonequilibrium conditions can be generated. In this context, microplasmas, or low-temperature plasmas confined to micrometer dimensions have emerged as a promising solution for a diverse range of problems in the field of advanced materials and devices. Here, we report recent progress in the field and discuss how microplasmas and their unique features facilitate synthesis of a broad range of nanomaterials and allow the fabrication of advanced light sources for materials analysis, lighting systems, active electromagnetic devices, and other commercial applications.

Microplasma applications are motivated by the demands of present-day fabrication of advanced materials with nanoscale features, especially in small reactor volumes and under conditions of fast flows, chemical microreactors, and atmospheric pressure.<sup>[1–4]</sup> Some of the persistent issues include specific and tunable properties such as size, surface-to-volume ratio, quantum confinement, and crystallinity of the nanomaterials


Prof. W.-H. Chiang  
Department of Chemical Engineering  
National Taiwan University of Science and Technology  
Taipei 10607, Taiwan

Prof. D. Mariotti  
Nanotechnology & Integrated Bio-Engineering Centre (NIBEC)  
Ulster University  
Shore Road, Newtownabbey BT37 0QB, UK

Prof. R. M. Sankaran  
Department of Chemical and Biomolecular Engineering  
Case Western Reserve University  
Cleveland, OH 44106-7217, USA

Prof. J. G. Eden  
Department of Electrical and Computer Engineering  
University of Illinois  
Urbana, IL 61801, USA

Prof. K. Ostrikov  
School of Chemistry  
Physics and Mechanical Engineering  
Queensland University of Technology  
Brisbane, QLD 4000, Australia  
E-mail: kostya.ostrikov@qut.edu.au

 The ORCID identification number(s) for the author(s) of this article can be found under <https://doi.org/10.1002/adma.201905508>.

© 2019 The Authors. Published by WILEY-VCH Verlag GmbH & Co. KGaA, Weinheim. This is an open access article under the terms of the Creative Commons Attribution License, which permits use, distribution and reproduction in any medium, provided the original work is properly cited.

DOI: 10.1002/adma.201905508

produced. In this regard, it is particularly challenging to synthesize small nanoparticles (NPs) because of their inherent tendency to form larger particles (i.e., aggregate or agglomerate).<sup>[5]</sup> For industrial applications, low-temperature operation at atmospheric pressure is crucial, especially for the large-scale (e.g., roll-to-roll) manufacturing processes. The unique size-dependent nonequilibrium features that are unique to microplasmas (compared to low-pressure plasmas and other atmospheric pressure plasmas) are of particular interest to the development of new technologies where both atmospheric pressure operation and small plasma size are essential, e.g., plasma printing in three dimensions or plasma-assisted additive manufacturing (3D plasma printing).

Here, we discuss how the essential features of microplasmas, such as thermal nonequilibrium, strong gradients, and some other properties help achieve exotic environments for the production of a broad range of nanomaterials of interest to energy, healthcare, chemical catalysis, and other applications. We also introduce the specific effects that make them indispensable for the development of sources of chemical agents and electromagnetic radiation, which can also be used in materials processing and analysis.

Microplasma applications in the development of materials and devices represent a relatively new field, with a clear trend of continuously increasing numbers of publications, intellectual property disclosures, and reported commercial applications. One of the reasons for this trend is the many possibilities to use such plasmas in synergy with gaseous, liquid, and mixed-phase media, electrochemical, hydrothermal, and several other methods. The plasmas help accelerate chemical reactions and bring the processes into the otherwise difficult to achieve parameter spaces. These and other complementary effects stimulate the notable recent developments in the field driven by numerous collaborative opportunities in materials-related areas. Not surprisingly, several reviews covering different aspects of low-temperature plasmas and applications have been published and received significant attention in multidisciplinary community. For example, the roadmap<sup>[6a]</sup> summarizes the progress and emerging trends in a much broader field of low-temperature plasma science and technology. Specific aspects related to nanomaterials processing, e.g., focusing on nanocrystal synthesis in the gas phase of low-pressure plasmas<sup>[6b]</sup> or insights into plasma-liquid interactions,<sup>[6c,d]</sup> have also been discussed. Plasma physics, discharge development, and plasma-focused technological aspects of microplasmas can be found in earlier<sup>[6e]</sup> and more recent<sup>[6f]</sup> reviews. However, since the earlier review<sup>[6g]</sup> and perspective<sup>[6h]</sup> articles, we are not aware of any recent progress reports dedicated to microplasma-assisted nanomaterials synthesis. Even though low-temperature plasmas have been recognized for the effective production and modification of electrode materials for renewable energy applications,<sup>[6i]</sup> this article focuses on recent progress in the area of microplasma-related materials and devices.

Complemented with the recent advances in microplasma sources of reactive species and radiation for materials processing and analysis, this Progress Report fills the obvious gap in the literature over the last 10 years, with the highlights of the latest advances over the last 3 years. A particular emphasis



**Wei-Hung Chiang** is an Associate Professor in the Department of Chemical Engineering, National Taiwan University of Science and Technology (NTUST), Taiwan. He received his Ph.D. from the Department of Chemical Engineering, Case Western Reserve University, USA in 2009. His research focuses on the synthesis, processing, and applications of functional nanomaterials. He also has broad scientific and engineering interests encompassing functional material design, synthesis and processing, device fabrication, and integration.



**Davide Mariotti** is a Professor of Plasma Science and Nanoscale Engineering with Ulster University in UK. He has previously worked internationally in Japan and USA and both in academic and industry. His research encompasses the design and development of innovative plasma-based processes to explore new materials opportunities. Concurrently to a strong application focus in photovoltaics and more broadly in energy applications, his research is also strongly driven by scientific discovery.



**Kostya (Ken) Ostrikov** is a Professor with Queensland University of Technology, Australia, a Founding Leader of the CSIRO-QUT Joint Sustainable Processes and Devices Laboratory, and Academician of the Academy of Europe and the European Academy of Sciences. His research focuses on nanoscale control of energy and matter contributes to the solution of the grand challenge of directing energy and matter at nanoscales, to develop renewable energy and energy-efficient technologies for a sustainable future.

is made on synergistic, complementary features of the plasmas that make them a versatile tool in materials-related applications.

We therefore examine the recent progress in microplasma-based synthesis of advanced nanomaterials, highlight the key features of microplasmas, and discuss salient examples of

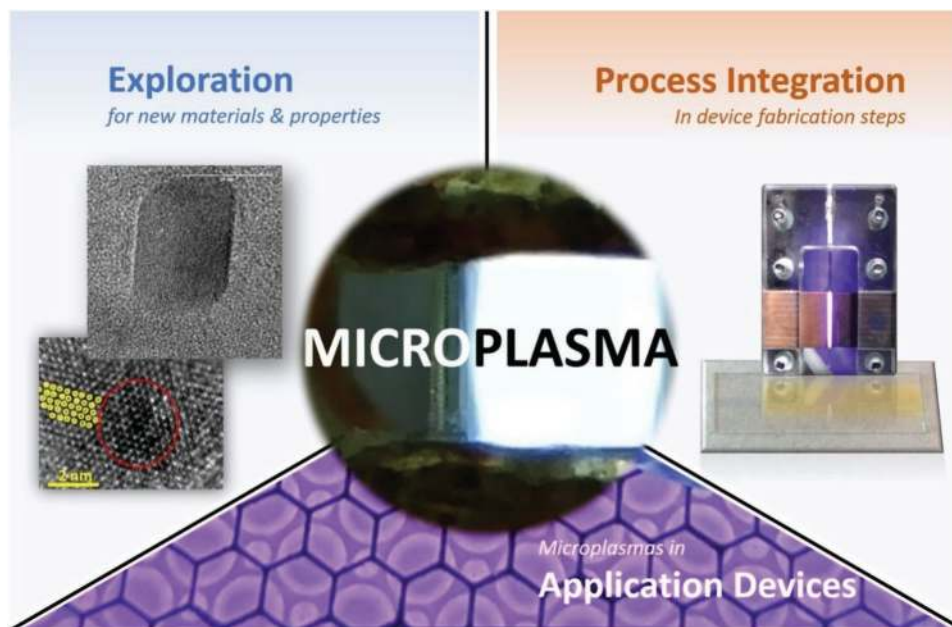


**Figure 1.** The scope and focus of this article. Three microplasma-related focus areas: fundamental research in nanoscale synthesis leading to new materials and functional properties, integration of the plasmas and plasma-processed materials into device fabrication processes, and microplasma applications in commercial devices and systems.

recent commercial applications. The key points of this Progress Report are summarized in **Figure 1**. Microplasmas represent a powerful approach for the “exploration” (top left segment, Figure 1) of new materials, overcoming thermodynamic stability and therefore achieving compositions and structures that are difficult or even impossible to achieve otherwise. Microplasma versatility allows “process integration” of the material synthesis into advanced device fabrication (top right segment, Figure 1), and utilizing these devices for materials analysis and other applications (bottom segment, Figure 1).

In Section 2 to follow, we discuss the unique general features of microplasmas that make them particularly suited for nanomaterials synthesis and other applications. Recent advances on the preparation of advanced nanomaterials using microplasmas are presented in Section 3. In Section 4, we highlight the existing and emerging commercial applications based on microplasmas. We conclude with Section 5, where future research needs and an outlook for applications of microplasmas in diverse materials-related fields are outlined.

## 2. Microplasmas: Key Features for Materials-Related Applications

### 2.1. Definition and Nonequilibrium

Microplasmas have emerged as unique active media for both nanomaterials production and operation of light sources and active chemical and electromagnetic devices. **Figure 2** shows schematics of representative electrode configurations including a microcavity reactor (Figure 2a), flow-through aerosol process (Figure 2b), film application (Figure 2c), and liquid-phase configuration (Figure 2d), and key properties of microplasmas

for nanoscale materials synthesis (Figure 2e). The high voltage (denoted as HV) can be applied to the electrodes (i.e., anode and cathode) to form plasmas using DC or radiofrequency (RF) power supplies with proper electrical circuits. The important effect of microscopic space where microplasma is confined is highlighted by the sketch in Figure 2a corresponding to microcavity plasmas. The microscopic confinement effects produce strongly nonequilibrium conditions, which in turn result in the specific conditions for nanomaterials synthesis, as discussed in Sections 2 and 3.5. The microplasma configurations (Figure 2a–d) have been successfully used for materials synthesis, especially for aerosol-like NP synthesis in the gas-phase, deposition of metal oxide nanostructures (NSs) and thin films, and colloidal dispersions of NPs. The examples of the materials synthesis and processing are presented in Section 3. Importantly, microplasmas represent a special class of “nonthermal” plasmas which are, as the name suggests, spatially confined to microscale dimensions.<sup>[7]</sup> “Nonthermal” refers to the lack of thermal equilibrium in these plasmas with the temperature of the background gas much lower than the temperature of the excited electrons. This is in contrast to thermal plasmas such as welding torches or even natural plasmas such as lightning where the temperature of the background gas is typically equal to the temperature of the excited electrons. Some other examples of nonthermal plasmas are neon lights for large space illumination and commercial signage. Other well-known nonthermal plasmas are low-pressure plasmas employed in thin-film etching, sputtering, and deposition applications, representing key processing steps in the microelectronic industry. Microplasmas differ from the low-pressure plasmas in that they can be operated up to and exceeding the atmospheric pressure, while avoiding thermal equilibrium despite having high power densities ( $>100 \text{ W cm}^{-3}$ ).<sup>[8]</sup> In other words, microplasmas can

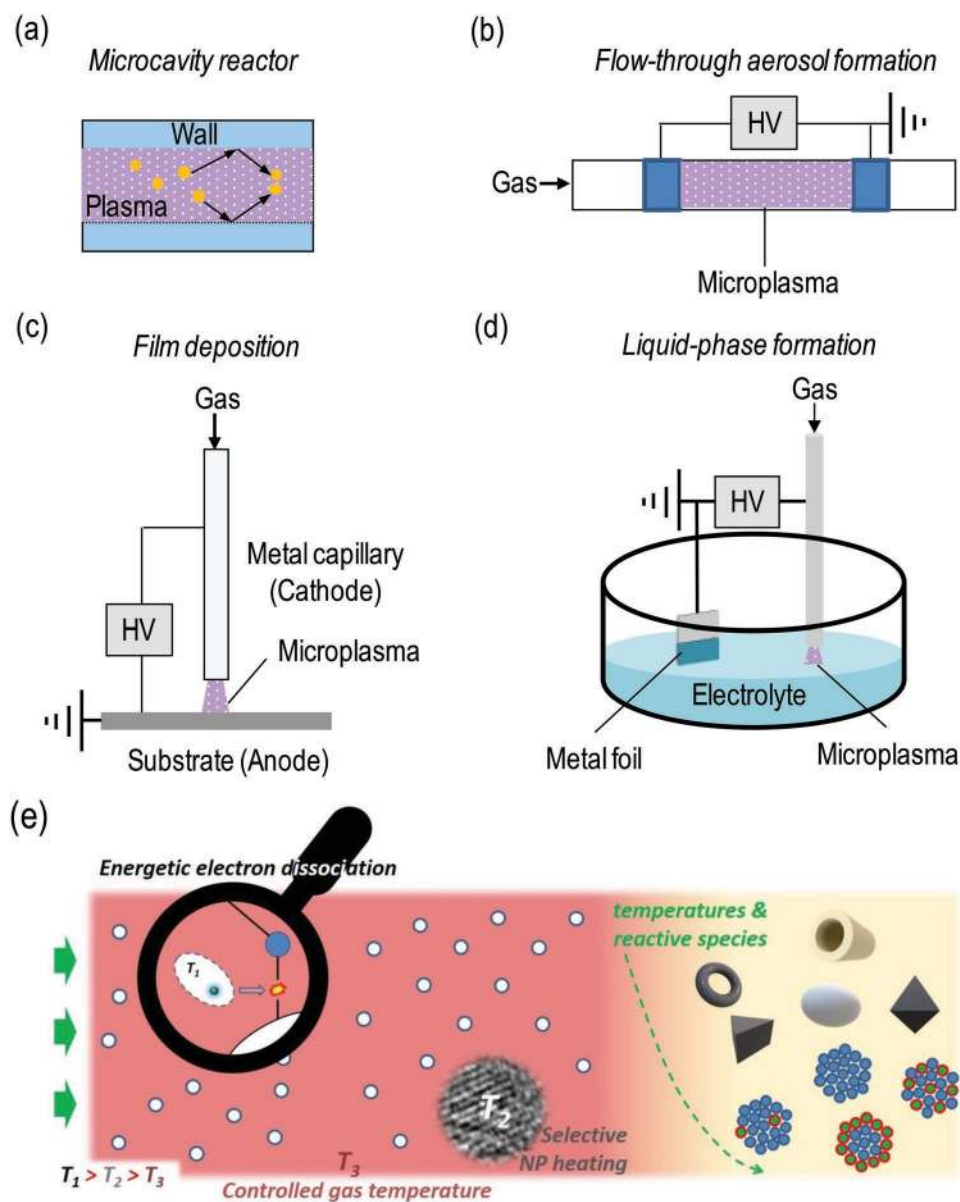


**Figure 2.** Principles of microplasma operation and applications for nanoscale materials synthesis. a–d) Schematics of representative microplasma configurations that have been successfully used for materials synthesis, including the microcavity reactor (a), flow-through aerosol formation (b), film deposition (c), and liquid-phase synthesis (d). HV denotes high voltage applied for microplasma generation. e) Schematic diagram representing a continuous-flow (left to right) synthesis process and distinctive features of microplasmas utilized in materials synthesis and processing. A microplasma is a highly reactive environment with radical species (white circles), which contribute to the synthesis of NPs and is characterized by a controlled gas temperature ( $T_3$ ), which can be as low as room temperature. Reactive species are produced by electron-induced dissociation. The electrons feature nonequilibrium energy distributions with high average energies. The high electron energies lead to reactions that would normally be achievable only at very high temperatures ( $T_1$ ). During the growth, NPs are subjected to selective heating, yet at a different temperature ( $T_2$ ). At the right-hand side of the microplasma, very strong gradients persist. These gradients cause effective quenching of chemical reactions often leading to the formation of nonequilibrium, metastable morphologies (e.g., NP shapes), and compositions that are difficult to achieve under thermodynamically equilibrium conditions.

be operated both at low and high pressures as opposed to typical atmospheric pressure or low-pressure plasmas.

## 2.2. Utility in Materials Processing

The physical characteristics of microplasmas translate into a wide range of fabrication options both in terms of materials

and device applications. For instance, low-temperature and atmospheric pressure processing conditions are compatible with soft materials such as polymers to avoid melting or vaporization. The gas temperature in a microplasma discharge could just exceed the glass transition temperature leading to diffusion and morphological changes. These conditions have also facilitated the coupling of microplasmas with a vast range of liquids such as water and alcohols, which is one of the most

recent developments in the field. These plasma–liquid systems have opened up a new field of research that blends plasma science, wet chemistry, electrochemistry, and physics (e.g., optical emission) of excited gases.<sup>[9]</sup> The combination of spatial confinement and gas flow has also led to short residence times in plasma reactors thus enabling sophisticated compositional tuning and phase stabilization of ultrasmall NPs.<sup>[10]</sup> The versatility of microplasmas is another important feature which has helped integrate the synthesized materials directly into devices by combining materials processing with device fabrication<sup>[11]</sup> or even incorporating the microplasmas themselves into the device.

### 2.3. Thermal Nonequilibrium: Challenge for Atmospheric Pressure Operation

The inherent “nonthermal” feature introduced above is useful for materials processing and active device operation because highly energetic reactions (e.g., leading to NP synthesis or active electromagnetic emission in light sources) can still take place while maintaining an overall low, near-room temperature processing environment. This feature helps overcome several persistent issues with the development of nonequilibrium plasmas that can be operated at atmospheric pressure. These plasmas are highly promising because they can be operated in a cost-effective way, e.g., without vacuum-related equipment, pump down time, etc. One of the main challenges with atmospheric pressure operation is the potential loss of nonequilibrium and the tendency for the plasma to experience a drastic increase in gas background temperature. In addition to the gas temperature increase, thermal equilibrium in plasmas also reduces the mean electron energy. The loss of high-energy electrons could be critical for applications in materials synthesis involving dissociation of relatively stable molecules such as nitrogen for the fabrication of nitride materials.

### 2.4. Effects of Microscale Confinement

Strategies to operate nonthermal plasmas at atmospheric pressure include tuning the power coupling such as nanosecond pulsing, designing the gas configuration such as afterglow jets, and enhancing the electron emission mechanisms, e.g., by using field emitting electrode materials. Among these, volume confinement to microscale dimensions has been one of the most effective and most popular approaches to achieve atmospheric pressure operation of nonequilibrium plasmas. The size of the plasma is critical to maintaining low, often near-room temperature, gas temperatures while producing electrons featuring nonequilibrium energy distributions. Simple energy balance calculations suggest that the small size enables effective cooling through the plasma surface so that gas heating is reduced even at high power densities that are created in the small volume.<sup>[6e]</sup> The electrode surface plays a key role when it has a large surface-to-volume ratio and can thus contribute to electron generation by secondary electron emission. The electrode configurations shown in Figure 2a–d can also create strong electric fields that augment electron excitation. For

instance, in a hollow (e.g., microcavity, Figure 2a) electrode configuration, electrons oscillate in the radial direction to increase collision rates, which is useful for the production of building units of advanced materials from gaseous precursors. With respect to the materials synthesis, a few *critical features* stand out among others, which are discussed below and visualized in Figure 2e.

### 2.5. Multi-Temperature Feature

A microplasma is a multi-temperature system with different species at different characteristic temperatures out of equilibrium with one another. For instance, when microplasmas are used for NP synthesis, the following temperatures could be tailored: the background process temperature, the temperature of the NPs being synthesized, and the precursor dissociation temperature. One distinctive feature of microplasmas versus low-pressure plasma is that the environment is much more sensitive to control parameters. In this case, if needed, the process temperature can be elevated well above room temperature by at least two orders of magnitude. For instance, a microplasma can be operated at  $\approx 400$  K background temperature,  $>700$  K NP temperature, and  $>10\,000$  K precursor dissociation temperature (electron temperature  $T_e$ ).<sup>[12,13]</sup>

### 2.6. Strong Gradients in a Microscale Reactor

The microscale dimensions have also introduced a distinct feature, which in some cases could be compared to the benefits found in the emerging field of microreactors.<sup>[14]</sup> For some microplasma-based processes, small reaction volumes directly translate into very short residence times thus offering the ability to quench building units and enhance materials nucleation processes. Furthermore, the plasma confinement owes to the electric rather than thermal effects, producing very strong gradients at the boundaries of the chemically active volume. Consequently, chemical reactions can be minimized just outside the reaction volume. These synthesis conditions help not only to arrest the growth of the particles at specific times (e.g., leading to ultrasmall sizes and narrow size distributions), but also to achieve metastable compositions and morphologies that are thermodynamically unstable but are kinetically accessible under nonequilibrium conditions.

### 2.7. Microplasmas versus Atmospheric Pressure Plasmas

The features related to the thermal and/or chemical nonequilibrium environments, generation of reactive species with energetic electrons, atmospheric pressure operation, usage of feedstock in various forms (liquid, solid, and gas), and some others are also possible to achieve in other types of atmospheric pressure discharges. However, gas-phase microplasmas (i.e., not interacting with liquids) exhibit a combination of key distinctive features compared to other plasmas operated at atmospheric pressure, which make them a most effective type of nonequilibrium atmospheric pressure plasmas

for synthesizing NPs in a flow geometry. A microplasma can sustain continuously high power densities across its full volume and with a wide range of gas mixtures and injected precursors, in some cases even with preformed NPs. These features all together are crucial to producing sufficient radical concentrations (over sufficient space and time) and background temperature that can lead to nucleation and growth of NPs. For instance, filamentary microdischarges, another type of atmospheric pressure plasmas, lacks the time- and space-continuity of radicals production which makes it difficult to nucleate NPs. Similar observations result from pulsed plasma operation when the ratio of on/off time is not sufficiently high. Other atmospheric pressure plasmas often lead to thermal instability and arcing when the gas mixtures required for NP synthesis are introduced. In some cases, e.g., where high gas flows are used to stabilize plasmas at atmospheric pressure, the residence time is drastically reduced limiting any possibility of nucleation and growth. In order to preserve a nonequilibrium environment amenable to NP nucleation and growth, the most effective solution is to enhance the cooling through plasma confinement in a small volume, i.e., sustain nonequilibrium atmospheric pressure plasmas in microscale volumes.

However, we should note that when plasmas are coupled with liquid, such critical features lose their significance and microplasmas somewhat act more similar to other atmospheric pressure plasmas. In these cases, the advantages of microplasmas are twofold. On one hand, microplasma allows in many cases better control and versatility both in terms of the accessible parameter space as well as in the practical aspects of implementing suitable configurations for materials synthesis and processing. The other aspect of practical interest relates to the possibility of microplasmas to accommodate the injection of liquid droplets in a flow configuration, which can be challenging or certainly with limited scope for other atmospheric pressure plasmas. It is worth mentioning that the metal NP production rates at a small laboratory scale ( $\approx 10^{23}$  atoms  $L^{-1} s^{-1}$ )<sup>[15]</sup> reported for this type of microplasmas are much higher not only compared to other plasma types but also compared to advanced chemical microreactors.

## 2.8. Process Versatility

The versatility of microplasmas for diverse materials processing and device applications cannot be overstated. First, the features discussed above make microplasmas an attractive reactive chemical environment for advanced materials synthesis as they offer a unique combination of synthesis conditions. Importantly, while initially microplasma development was largely motivated by atmospheric pressure operation, such plasmas can also be operated at low (vacuum) pressures.<sup>[16]</sup> We emphasize that microplasmas can be generated with DC, AC, RF, pulsed, and other excitations, a wide range of gases and vapors such as Ar, He, N<sub>2</sub>, and air, gas flow, diverse electrode geometries, and materials. The scale of microplasma experiments also ranges from portable and benchtop devices to arrays aimed for digital manufacturing. Together, these reasons have led to a strong expansion of microplasma applications requiring nonequilibrium, atmospheric pressure operation. One such application

area is the production of advanced materials. The selected examples representing the most notable progress in the field over the last decade present different means of microplasma-enabled synthesis of nanomaterials in the gas and liquid phase, in both free-standing and substrate-supported forms.

## 2.9. Microplasma Enabled Devices

Other rapidly expanding areas of microplasma applications discussed here are the development of next-generation optoelectronic devices, water sterilization systems, powerful UV light sources, and active electromagnetic devices. These applications are also enabled by the unique microplasma properties and their interactions with functional materials. Indeed, microplasmas are efficient generators of charged and electrically excited atoms and molecules, largely because of their nonequilibrium nature. Strong nonequilibrium between the gas and electron temperatures allows effective control over the distribution of chemical products generated by electron impact excitation of gases maintained at temperatures as low as room temperature.

## 2.10. High-Power-Density, Low-Temperature Operation

In both types of (materials and devices) applications, operation of microplasmas at *very high power densities* is useful (and often critical). The reason is because the internal energy of the many atomic and molecular excited species (such as rare gas metastables) is higher than needed to liberate a desired atom from a parent molecule through collisional excitation transfer. It is also possible to control the number densities and mixing of multiple-phases of excited and ionized atoms and molecules including metastable species and products of diatomic and polyatomic molecule dissociation that are unprecedented in many thermal and other plasma-based processes. Furthermore, the atmospheric pressure (and above) operation typical of microplasmas offers an avenue for the generation of additional products through collisions of the nascent fragments (i.e., produced directly by electron impact excitation, ionization, or dissociation) with the background gas(es). Consequently, microplasma-driven materials synthesis and processing is able to proceed at temperatures considerably lower than those required by processes relying on thermal equilibrium, such as metal-organic chemical vapor deposition (CVD), to dissociate, e.g., polyatomic molecular precursors.

With these key features in mind, we can now proceed with the analysis of the recent progress in microplasma-assisted synthesis and modification of advanced nanomaterials.

## 3. Production of Advanced Nanomaterials

Recent years have witnessed major advances in the fabrication of advanced nanomaterials using microplasma-assisted gas phase and liquid phase approaches. Selected examples include ultrasmall metal NPs (USMNP) in Section 3.1, semiconductor NPs (SNPs) in Section 3.2, metal oxide nanostructures

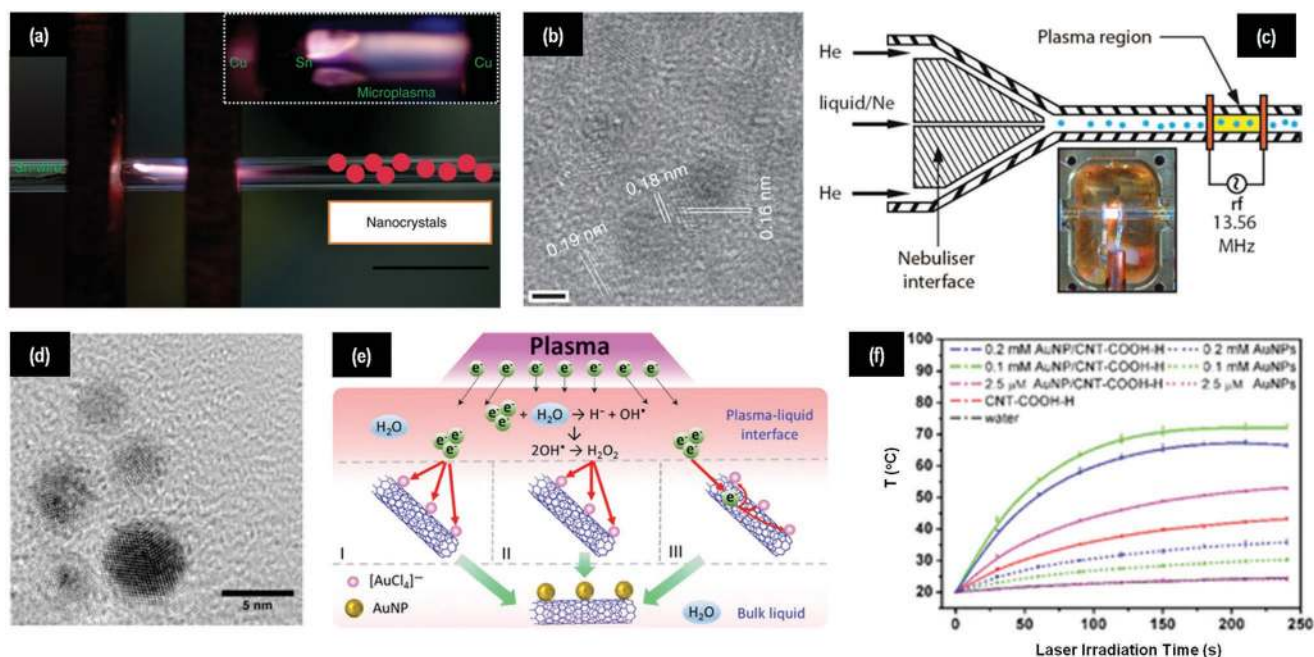


**Figure 3.** Microplasma synthesis of ultrasmall metallic NPs. a) Microplasma reactor for Sn NP synthesis. A thin tin wire as the Sn precursor is used in the microplasma reactor. Inset shows the image of the microplasma. Scale bar: 4 mm. b) HRTEM image of Sn NPs synthesized in the microplasma reactor shown in (a) with average diameter of 1.6 nm. Scale bars: 2 nm. a,b) Reproduced under the terms of the CC-BY Creative Commons Attribution 4.0 International License (<http://creativecommons.org/licenses/by/4.0/>).<sup>[26]</sup> Copyright 2018, The Authors, published by Springer Nature. c) Schematic representation of the droplet-plasma microreactor for Au NP synthesis. Inset shows the photograph of the ignited plasma region. d) HRTEM image of Au NPs synthesized by a droplet-plasma microreactor shown in (c). c,d) Reproduced with permission.<sup>[15]</sup> Copyright 2018, American Chemical Society. e) Proposed reaction mechanism of AuNP/CNT nanocomposites synthesized by microplasma-liquid method. f) Photothermal properties of as-prepared AuNP/CNT nanocomposites synthesized with different HAuCl<sub>4</sub> concentrations in microplasma-liquid method. e,f) Reproduced with permission.<sup>[38]</sup> Copyright 2019, American Chemical Society.

(MONS) in Section 3.3, and carbon nanomaterials (CNMs) in Section 3.4. Section 3.5 is devoted to the discussion of the benefits of using microplasmas in the processing of nanomaterials that can complement and diversify the existing approaches. Examples of microplasma-assisted synthesis of USMNPs include catalytic, transition metals such as Ni, Fe, NiFe, NiFeCu, and Sn as well as plasmonic Ag, Au, and AgAu. Examples of semiconducting materials include Si, SiC, CdS, Sn-doped CdS, and Co<sub>3</sub>O<sub>4</sub>, NPs. Metal oxides are represented by CuO, NiO, and Fe<sub>2</sub>O<sub>3</sub> films and In<sub>2</sub>O<sub>3</sub>, Cu<sub>2</sub>O, Y<sub>2</sub>O<sub>3</sub>, and doped Y<sub>2</sub>O<sub>3</sub> NPs. The examples of CNMs include carbon dots (CDs), graphene quantum dots (GQDs), nanographene, and nanodiamonds (NDs).

### 3.1. USMNPs

Recent theoretical and experimental studies suggest that USMNPs ranging from 1 to 5 nm in diameter exhibit exceptional properties and are desired for energy conversion and storage, optoelectronics, nanoelectronics, catalysis, bioimaging, and biomedical applications.<sup>[5a,17,18]</sup> Their properties are highly sensitive to both the size and chemical composition of the particles. However, it is currently challenging to synthesize well-dispersed, free-standing particles due to the poor stability and severe aggregation resulting from their high surface free energy. On the other hand, various supports

including 2D layered materials, nanoporous materials, metal oxides, and polymers have been proposed to stabilize the USMNPs.<sup>[5a]</sup>

Microplasma synthesis has been reported as a promising and effective method to synthesize free-standing USMNP without significant aggregation.<sup>[6]</sup> In general, microplasma-assisted NP synthesis can be classified into the gas-phase and liquid-phase approaches.<sup>[6]</sup> Recently, transition metal USMNPs have been demonstrated with potential applications for materials fabrication, catalysis, energy conversion, and storage.<sup>[5a,17,18]</sup> Representative examples of microplasma-assisted metal NP synthesis are presented in **Figure 3**. In gas-phase microplasma-assisted synthesis, vapors of metal-organic precursors are typically introduced in the plasma using a carrier gas flow. The metal-organic precursor is dissociated in the plasma and the resulting metal radicals nucleate to form metal clusters into metal particles.<sup>[19]</sup> Multiple metal-organic precursors can be mixed to produce bimetallic<sup>[20]</sup> and trimetallic NPs.<sup>[21]</sup> Indeed, ultrasmall Ni, Fe, NiFe bimetallic, and NiFeCu trimetallic NPs with diameters ranging from 2 to 5 nm and relatively narrow size distributions ( $\sigma < 20\%$ ) have been demonstrated using atmospheric pressure DC microplasmas.<sup>[19–23]</sup> The size and composition of NiFe bimetallic NP catalysts has been shown to assist controlling the diameters and chiralities of the single-walled carbon nanotubes (CNTs) during the growth.<sup>[23]</sup> Further, the size distribution, morphology, crystal facet structure, and magnetic properties of the Ni and iron oxide NP synthesized by

gas-phase microplasmas can be affected by the plasma conditions and precursor concentration.<sup>[24,25]</sup> Recently, the synthesis and properties of surfactant-free, free-standing ultrasmall Sn NPs with diameters ranging from 1.6 to 6.1 nm, were reported (Figure 3a).<sup>[26]</sup> The produced Sn NPs exhibit high crystallinity and purity (Figure 3b) and possess excellent electrochemical capacity for emerging energy storage devices such as microsupercapacitors.

Plasmonic NPs such as Ag, Au, and AuAg bimetallics are actively pursued for biosensing, nanocatalysis, and biomedical applications.<sup>[27–29]</sup> However, common synthesis methods, e.g., based on wet-chemistry, suffer additional reducing and capping agents and generally involve laborious multistep processes. A simple method to prepare Au NPs by employing a H<sub>2</sub>/Ar microplasma jet driven with ultrahigh frequency at ambient pressure was shown very effective and was followed by other researchers.<sup>[30]</sup> The synthesized Au NPs with 4.3 nm average size can be directly deposited on temperature-sensitive substrates such as paper at ambient conditions without any apparent damage. This ability is promising for the development of plasma printing applications. Reducing-agent-free, rapid production of colloidal Ag, Au, and AgAu alloy NPs is possible using microplasma-assisted electrochemical synthesis.<sup>[31–36]</sup> The absorbance spectroscopic studies indicate that particle nucleation and growth are possibly initiated by the plasma-liquid interactions.<sup>[31]</sup> A facile and green synthesis of crystalline AuAg NP alloys has been demonstrated in solution under ambient conditions. In this method, it is possible to control the elemental composition and the size of the NPs by varying the reaction time.<sup>[36]</sup> A DC atmospheric pressure glow microdischarge produced Au-Ag core-shell NPs (Au@Ag CSNPs) using a continuous flow reactor.<sup>[37]</sup> This work exhibits a production rate of 90 mL h<sup>-1</sup> for a Au@Ag CSNP solution. An interesting example of continuous-flow synthesis of ligand-free colloidal Au NP with the average size of 4 nm, was demonstrated using micro-droplets passing through the plasma generated in a narrow channel (Figure 3c).<sup>[15]</sup> Importantly, nonequilibrium and high energy density conditions lead to nearly complete precursor reduction. Moreover, the as-synthesized NPs were dispersed in solution and free of surfactants and ligands on the surfaces, making them potentially useful for applications including drug delivery, biomedical imaging, and catalysis (Figure 3d).

Besides free-standing NPs in gas phase or colloidal NPs dispersed in solution, nanocomposites or nanohybrids composed of metal NPs and substrate materials including CNT, graphene nanosheets, polymers, and hydrogels can be prepared using microplasma-assisted liquid-phase synthesis at room temperature and ambient pressure. Recent works include AuNP/CNT,<sup>[38]</sup> AuNP/graphene oxide (GO),<sup>[39]</sup> AuNP/poly(3,4-ethylenedioxythiophene) polystyrene sulfonate,<sup>[40]</sup> and Fe<sub>3</sub>O<sub>4</sub>NP/poly(*N*-isopropylacrylamide) hydrogels.<sup>[41]</sup> For example, Au NPs can be directly synthesized from Au containing salt precursor by chemical reduction and simultaneously deposited on CNT surfaces to form a nanohybrid-like structure during the microplasma-assisted liquid-phase synthesis (Figure 3e). The study indicates good photochemical properties of these nanocomposites for potential therapeutic applications (Figure 3f).<sup>[38]</sup>

### 3.2. Semiconducting Materials

SNPs are important materials for optoelectronics, bioimaging, energy conversion, quantum computing, and other areas.<sup>[42,43]</sup> Microplasmas have been used to synthesize Si and other semiconducting NPs with controlled morphologies and properties with typical examples presented in Figure 4. The early microplasma-based synthesis of Si NPs relied on mixtures of SiH<sub>4</sub> and Ar gases and DC power.<sup>[44]</sup> The prepared Si particles possessed diameters from 2 to 5 nm and exhibited a 420 nm photoluminescence (PL) emission at ambient temperature. Si NPs were later prepared by operating a very high frequency microplasmas in H<sub>2</sub>, Ar, and SiCl<sub>4</sub> gas mixtures.<sup>[45]</sup> Importantly, the H<sub>2</sub> concentration was found to affect the synthesis rates and the optical properties of the Si NPs. Si NPs with high crystallinity and distinctive shapes can be synthesized without H<sub>2</sub> addition to the Ar and SiH<sub>4</sub> gas mixture when RF microplasmas are used. Moreover, the PL emissions of the Si NPs can be tuned in the visible range by adjusting the H<sub>2</sub> concentration.<sup>[46]</sup> Recently, it has been reported that Si NPs can also be synthesized by microplasma-assisted liquid-phase processing at ambient conditions.<sup>[47]</sup> Moreover, microstructured SiO<sub>x</sub> thin films can be deposited from hexamethyldisilazane and hexamethyldisiloxane precursors using microplasma jet under ambient pressure,<sup>[48]</sup> showing the potential of microplasmas for semiconductor materials synthesis.

Silicon carbide (SiC) is a versatile material which is very hard, chemically inert, and is promising for next-generation photonic and electronic devices.<sup>[49–51]</sup> The current synthesis of SiC NPs, however, is very difficult because of the hardness and high melting temperature of bulk SiC. Recently, highly crystalline and ultrasmall SiC NPs with the particle size less than 1.5 nm and ligand-free surface were synthesized using gas-phase atmospheric pressure microplasmas.<sup>[52]</sup> Transmission electron microscopy (TEM) results confirm that free-standing SiC nanocrystals with clear shapes and diameters ranging from 1.5 to 5.3 nm can be produced by microplasmas without any additional surface treatment (Figure 4a,b).

Recently, liquid-phase microplasma-assisted synthesis of semiconducting NPs has been demonstrated. For example, cadmium sulfide (CdS) NPs can be effectively synthesized by microplasma-liquid processing using solutions containing CdSO<sub>4</sub>, Na<sub>2</sub>S<sub>2</sub>O<sub>3</sub>, and thioglycolic acid (Figure 4c,d).<sup>[53]</sup> The as-prepared CdS NPs exhibit stable room-temperature PL properties. Interestingly, Sn-doped CdS NPs can be prepared using a similar method by adding SnCl<sub>4</sub> in the solution, leading to better PL performance (Figure 4e).<sup>[54]</sup> Moreover, CdS-Ag<sub>2</sub>S on GO nanocomposites were recently synthesized using microplasma-assisted liquid-phase method.<sup>[55]</sup>

### 3.3. MONS

MONS is an important class of materials because they can be custom-designed to produce insulating, semiconducting, or even conducting properties by controlling the basic structure of the M-O-M network.<sup>[56]</sup> MONS are highly promising for various applications including photoelectric energy



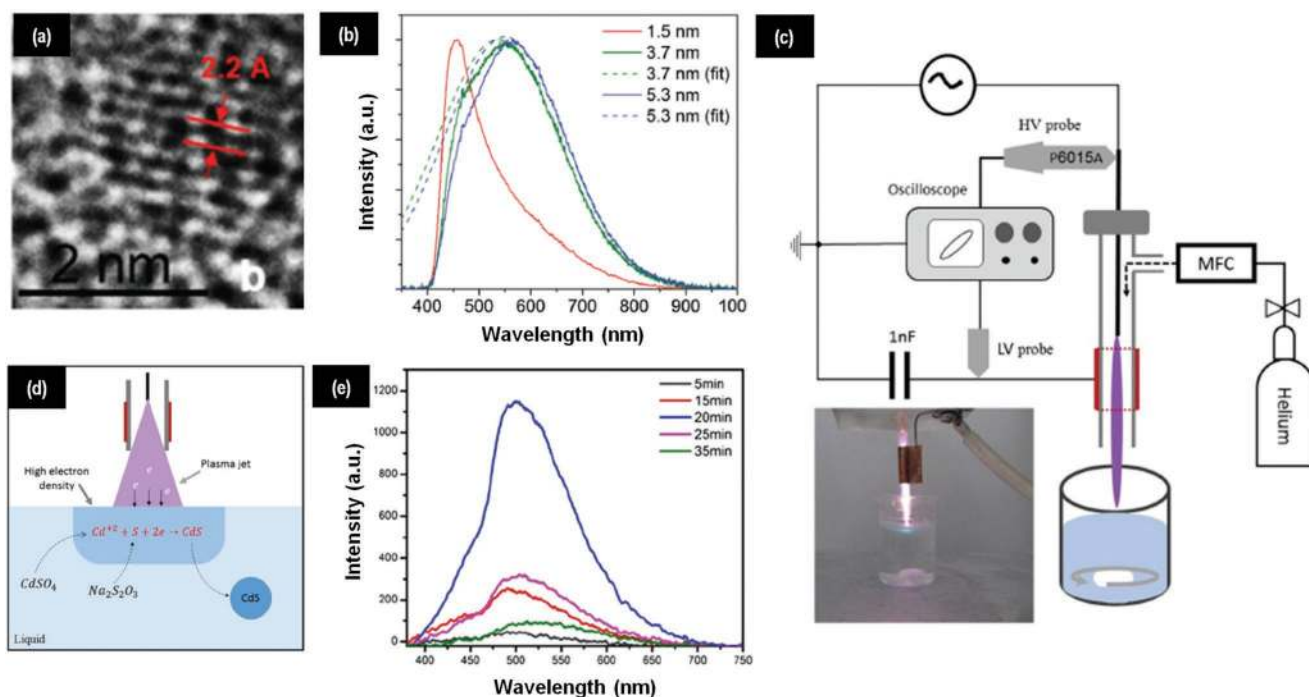


**Figure 4.** Microplasma synthesis and doping of semiconducting NPs. a) HRTEM image of a highly crystalline SiC NP synthesized using gas-phase microplasmas. b) PL spectra of SiC NPs with different particle size controlled by the synthesis conditions in the microplasma reactor. a,b) Reproduced with permission.<sup>[52]</sup> Copyright 2016, The Royal Society of Chemistry. c) Schematic of the experimental setup of CdS NP synthesized using microplasma-assisted liquid phase synthesis. d) Proposed chemical pathway of CdS NP synthesis using microplasma-assisted liquid phase synthesis. e) PL spectra of CdS NPs produced using a microplasma reactor as shown in (c), with varied synthesis time. c–e) Reproduced with permission.<sup>[53]</sup> Copyright 2017, Springer Nature.

generators, sensing devices, optoelectronic, spintronic, and electronic devices.<sup>[56–59]</sup> Current synthesis methods of MONS include gas-phase techniques such as sputtering, laser deposition, atomic layer deposition (ALD), and thermal deposition. Common solution processing methods include dip coating, spin-coating, and spray pyrolysis. However, some of the existing methods suffer from the use of expensive vacuum systems, low deposition rates, high-temperature (e.g., above 400 °C) annealing, and multiple process steps. Other common issues include poor materials quality due to the product segregation during annealing process.<sup>[58]</sup> Another critical challenge is to achieve direct-patterned MO structures with controlled material composition at the nanoscale on a wide range of substrates at low process temperatures.

Recently, a versatile microplasma-based approach (**Figure 5**) has been demonstrated for direct deposition of crystalline MONS including  $\alpha$ -Fe<sub>2</sub>O<sub>3</sub>, CuO, NiO, and Fe-doped NiO on different substrates including polymeric materials, conductors, insulators, fibers, and patterned substrates at ambient temperature (Figure 5a).<sup>[16,60–62]</sup> The as-prepared CuO films were used as active electrodes for lithium ion batteries, exhibiting high specific capacity and good electrochemical responses over a large number of voltage sweep cycles (Figure 5b). The microplasma deposition can also be applied for conformal single-step deposition of  $\alpha$ -Fe<sub>2</sub>O<sub>3</sub> (Figure 5c), NiO (Figure 5d), and Fe-doped NiO (Figure 5e) materials. Moreover, it is possible to perform large area deposition by raster scanning a single microplasma jet, which is potentially suitable for plasma printing applications.

Recently, vertically oriented nanosized NiO structures encapsulated in graphene layers (G@NiO) were prepared by microplasma-enhanced CVD.<sup>[63]</sup> Pt/ZnO nanocomposites were fabricated as counter electrodes of dye-sensitized solar cells using nitrogen DC-pulsed atmospheric pressure microplasma jet in a few seconds due to the highly reactive species generated in the nitrogen plasma.<sup>[64]</sup>

Metal oxide NPs can also be prepared using liquid-phase, microplasma-assisted approach. The plasma–liquid interface can be a reaction hot zone because of the active species such as electrons, ions, excited OH, metastable Ar, and nitrogen-related species produced by the plasma. A microplasma-liquid method was designed to synthesize cuprous oxide (Cu<sub>2</sub>O) NPs with the size ranging from 400 to 600 nm.<sup>[65]</sup> It was further demonstrated that crystalline Co<sub>3</sub>O<sub>4</sub> NPs with the diameters 2–5 nm can be fabricated by using Co foil as the anode in the microplasma-enhanced electrochemical reactor operated at ambient conditions.<sup>[66]</sup> The Co<sub>3</sub>O<sub>4</sub> NPs produced in this method can be dispersed in ethanol and then used to fabricate thin films for light absorption and light-emitting diode applications.

Indium oxide In<sub>2</sub>O<sub>3</sub> with a relatively wide bandgap of about 3.0 eV is very useful for many applications including solar energy conversion, sensing devices, photochemical reactions, and optoelectronic devices.<sup>[67,68]</sup> In<sub>2</sub>O<sub>3</sub> NPs were successfully fabricated using microplasma-liquid processing.<sup>[69]</sup> The optical properties of the NPs can be controlled by adjusting the plasma synthesis time and precursor concentrations (Figure 5f).<sup>[69]</sup>

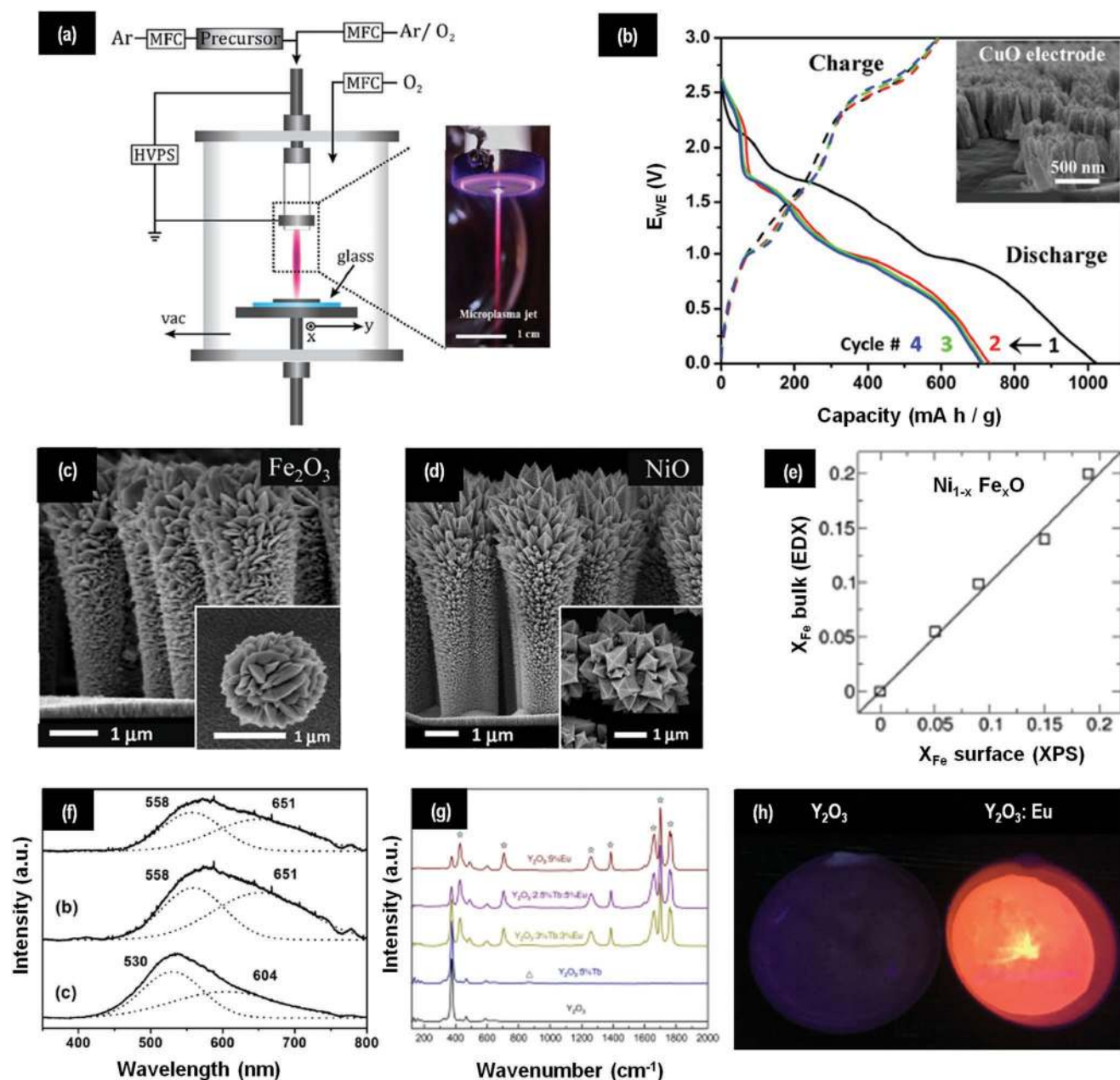


**Figure 5.** Microplasma fabrication of MONS. a) Schematic of microplasma-enhanced synthesis and deposition of MONS on varying substrates. b) Electrochemical discharge–charge measurement for lithium ion battery anode using CuO film deposited on Cu foil by the method in (a). Inset shows the scanning electron microscopy image of the CuO film. c)  $\alpha$ -Fe<sub>2</sub>O<sub>3</sub> and d) NiO deposited on 2.5  $\mu$ m high Si micropillars by the method presented in (a). The insets show top-down zoom images of the oxide morphology. a–d) Reproduced with permission.<sup>[60]</sup> Copyright 2016, American Institute of Physics. e) Comparison of surface and bulk compositions of Ni<sub>1-x</sub>Fe<sub>x</sub>O films obtained via X-ray photoelectron spectroscopy and energy-dispersive X-ray spectroscopy, respectively, where  $x = [\text{Fe}] / ([\text{Fe}] + [\text{Ni}])$  and  $[\text{Fe}]$  and  $[\text{Ni}]$  denote concentrations of Fe and Ni, respectively. Reproduced with permission.<sup>[62]</sup> Copyright 2017, Royal Society of Chemistry. f) PL spectra of cubic In<sub>2</sub>O<sub>3</sub> NPs synthesized with varying time using microplasma-assisted liquid phase method. Reproduced with permission.<sup>[69]</sup> Copyright 2016, American Chemical Society. g) Raman spectra of Eu- and Tb-doped Y<sub>2</sub>O<sub>3</sub> NPs synthesized using microplasma-assisted liquid phase method. Reproduced with permission.<sup>[76]</sup> Copyright 2019, Wiley-VCH. h) Photographs of the synthesized Y<sub>2</sub>O<sub>3</sub> and Y<sub>2</sub>O<sub>3</sub>:5% Eu samples in the aqueous solution under room light and UV irradiation (254 nm). Y<sub>2</sub>O<sub>3</sub>:5% Eu sample shows a strong red-orange fluorescence. Reproduced with permission.<sup>[77]</sup> Copyright 2019, The Royal Society of Chemistry.

Yttrium oxide NPs is one of the air-stable luminescent materials pursued for optoelectronics.<sup>[70,71]</sup> Additionally, the lanthanide (La)-doped yttrium oxide NPs have been reported as a low-toxicity luminescent material for biomedical applications.<sup>[72–74]</sup>

Yttrium oxide NPs have been successfully produced in a simple microplasma-assisted liquid process operated at ambient pressure by reacting yttrium nitrate aqueous solution as the precursor (Figure 5g).<sup>[75]</sup> Furthermore, successful synthesis of

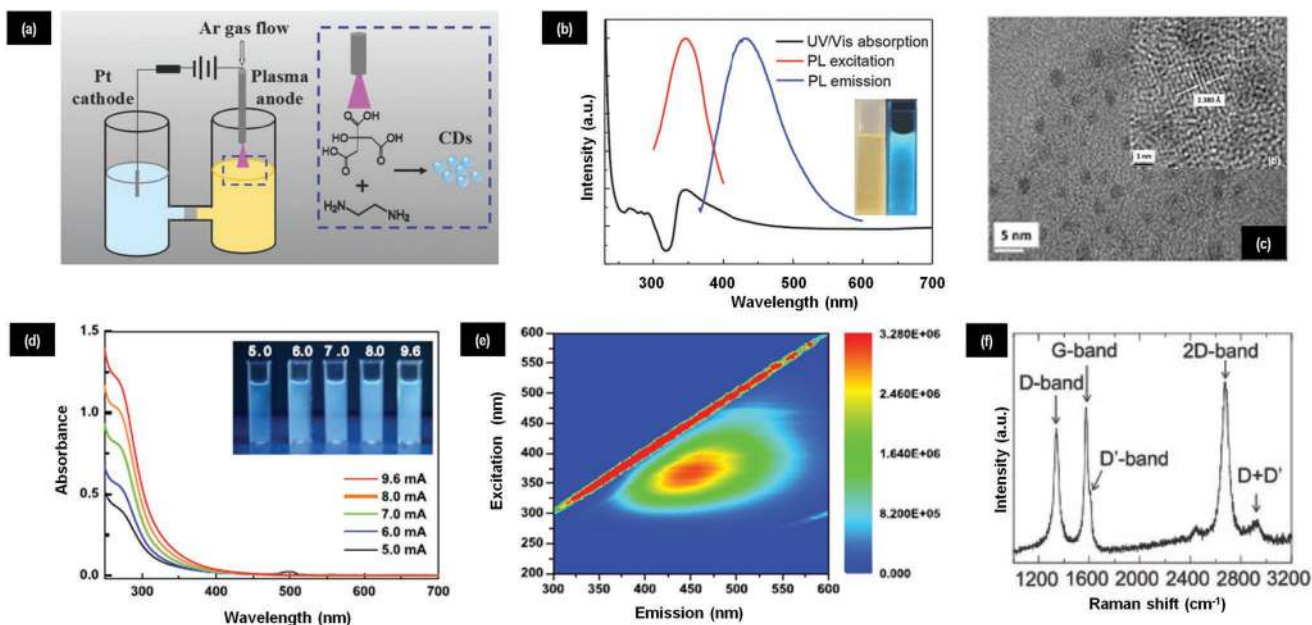


**Figure 6.** Microplasma synthesis of CNMs. a) Schematic of synthesis of CDs using microplasma-assisted liquid-phase method. b) UV-vis absorption, PL excitation, and PL emission spectra (Ex = 350 nm) of CDs in aqueous solution. The inset shows the photos of CDs under sunlight (left) and 365 nm UV light (right). a,b) Reproduced with permission.<sup>[94]</sup> Copyright 2014, The Royal Society of Chemistry. c) TEM of CDs produced by microplasma-assisted liquid phase method. The inset shows the HRTEM of a CD with the lattice spacing corresponding to (531) crystalline plane. Reproduced with permission.<sup>[95]</sup> Copyright 2015, Wiley-VCH. d) UV-vis absorption spectra of colloidal GQDs synthesized with varying process current using microplasma-liquid method. The inset shows the photos of as-produced colloidal GQDs under 365 nm UV lamp illumination. e) Photoluminescence mapping of as-produced colloidal GQDs in (d). Reproduced with permission.<sup>[99]</sup> Copyright 2019, Elsevier. f) Raman spectrum of nanographene produced by microplasma-assisted liquid-phase synthesis from ethanol with *N,N*-dimethylformamide-solvated FePc. Reproduced with permission.<sup>[107]</sup> Copyright 2018, Institute of Physics and The Japan Society of Applied Physics.

crystalline Eu, Tb, and lanthanide (La) single-doped and co-doped yttrium oxide NPs has been reported (Figure 5h).<sup>[76,77]</sup> Optical spectroscopy studies indicate that the PL emission properties can be adjusted by the dopant concentrations in the yttrium oxide NPs, which in turn can be controlled by the plasma process conditions. Other MONS including ZnO nanosheets,<sup>[78,79]</sup> TiO<sub>2</sub> nanotube,<sup>[80]</sup> europium-doped ceria NPs CeO<sub>2</sub>,<sup>[81]</sup> CuO NPs,<sup>[82,83]</sup> CuO/TiO<sub>2</sub> nanocomposite,<sup>[84]</sup> Ag/TiO<sub>2</sub> nanocomposite,<sup>[85]</sup> SnO/GNS nanocomposite<sup>[86,87]</sup> were recently synthesized using the microplasma-assisted liquid-phase method. These results confirm high potential of microplasmas in oxide materials processing and deposition for optoelectronics, sensing, and energy applications.

### 3.4. CNMs

CNMs including graphene, GQDs, CDs, and NDs, are emerging nanomaterials for chemical and biosensing, energy conversion, catalytic, medical imaging, and optoelectronic devices due to their exceptional properties including tunable bandgap, PL emission, and biocompatibility.<sup>[88–90]</sup> Current synthesis methods such as top-down and bottom-up approaches are usually time-consuming and laborious, and require high temperatures, as well as toxic precursors and chemicals.<sup>[90–93]</sup> Microplasma-assisted synthesis including gas-phase and liquid-phase approaches can be versatile and effective in the controlled production of CNMs, with typical examples presented in Figure 6.

CDs can be produced within just a few minutes using a microplasma-liquid method without high temperature condition, large energy input, and laborious procedures.<sup>[94–101]</sup> The plasma-assisted reactive chemistry promotes chemical reactions and accelerates the CDs formation. The synthesized CDs show a mean particle size of 2.3 nm and carbonyl and amide functionalities on the surface (Figure 6a,b).<sup>[94]</sup> The CDs can be used for pH sensing in the range of 3–14 and uranium detection with a high selectivity and low detection limit because of the stable luminescence properties under low pH and high salt concentration conditions.

Another example of a plasma-assisted liquid-phase process is the fast, environmentally friendly synthesis of blue-luminescent CDs with a mean size of 2.4 nm at ambient conditions.<sup>[95]</sup> The PL study shows that the emission peak of CDs can be tuned from 443 to 456 nm with varying excitation wavelength from 360 to 410 nm (Figure 6c). Environmentally friendly synthesis of CDs from folic acid (FA) is further achieved using microplasmas.<sup>[96]</sup> The produced FA CDs show the excitation independent emission near 445 nm. The fluorescence quantum yield is estimated to be 13% under 370 nm excitation. The synthesized CDs were used in bio-imaging by fluorescence labeling of MCF-7 cancer cells. Colloidal GQDs have been recently produced in aqueous solutions using microplasma-assisted liquid-phase synthesis at ambient conditions (Figure 6d,e).<sup>[99]</sup> In this work, the colloidal GQDs were highly stable in solution and exhibited room-temperature PL emission at 448 nm. The obvious advantages of the microplasma-based synthesis are it is

simple, fast, and requires no additional reducing chemicals nor strong acids or bases.

Ultrafast synthesis of graphene structures with high quality was demonstrated using nonequilibrium, atmospheric pressure microplasma with a high electron density and alcohols or other hydrocarbons as the carbon precursor.<sup>[102–107]</sup> Few-layer nanographene structures with reasonable crystallinity can be obtained using this method according to the Raman analysis presented in Figure 6f. Moreover, N-doped nanographene can be synthesized using gas-phase microplasmas at ambient pressure with ethanol and ammonia as carbon and nitrogen precursors.<sup>[108]</sup>

Diamond, a metastable form of carbon, is difficult to synthesize at ambient conditions. Diamond films are commonly fabricated by low-pressure plasma-enhanced CVD due to the generation of atomic hydrogen. Atomic hydrogen species are important in stabilizing the diamond surface and suppressing the growth of nondiamond phases. According to theoretical calculations, it is suggested that carbon clusters with size less than 3 nm and hydrogen surface terminations are thermodynamically more stable in the form of  $sp^3$  hybridization than the  $sp^2$  forms. This calculation suggests that microplasmas can indeed be a suitable technology to synthesize ND under nonequilibrium, yet reasonably close to ambient conditions. Recently it has been demonstrated that NDs can be synthesized in microplasma-based processes.<sup>[109–112]</sup> Specifically, NDs have been synthesized using a DC microplasma and ethanol as a precursor.<sup>[109]</sup> NDs with 2–5 nm in diameter and high purity and crystallinity can be prepared by adding  $H_2$  gas to the gas mixture. The high quality and ultrasmall size of the NDs are particularly valuable for biomedical applications.<sup>[90]</sup>

An RF microplasma jet generated at atmospheric pressure can be used to synthesize other types of carbon microstructures including diamond particles, carbon nanowires, and CNTs by adjusting the deposition parameters such as the flow rate of precursors, the geometry of the electrode, and the substrate conditions.<sup>[113]</sup> Carbon nanowires and CNTs are promising materials for applications in electronics, as modified electrodes in chemical and biosensing, as well as energy storage applications.<sup>[114,115]</sup>

### 3.5. Microplasma Features that Diversify and Complement Existing Materials Synthesis

There are several features that microplasmas exhibit for the synthesis of various nanomaterials that diversify and complement existing approaches and methods. In some cases, these features could be regarded as advantageous and could be used by materials scientists and engineers. Below we highlight some of the most important features that were useful in the above examples of nanomaterials synthesis in Sections 3.1–3.4. We relate these results to the general features of microplasmas introduced in Section 2.

**NP Size Tunability:** In general, microplasmas possess a microreactor geometry and, analogously, are characterized by very short reaction residence times ranging from  $\mu s$  to ns that underpin the synthesis of ultrasmall (<5 nm in diameter) particles discussed in Section 2.6. However, whereas tuning

of the particle size has been demonstrated by varying the residence time in liquid-phase microreactors and low-pressure continuous plasmas with larger residence times, evidence of such control in microplasmas is presently limited. A possible reason is that there are coupled effects, e.g., if the residence time is decreased to decrease the particle size by increasing the gas flow rate, the gas temperature also decreases because of convective cooling, which could lead to enhanced particle nucleation and, in direct opposition, an increase in particle size. In other cases, where residence time does seem to control the size, other particle features also may change as a result of a cooler microplasma, i.e., chemical composition, crystal structure, and morphology may also change. Other “knobs” available to vary the residence time could also have coupled effects. Moreover, the gas flow rate could also affect the fluid properties, which unlike a liquid, will transition from a laminar to turbulent flow regime. To date, the most successful approach to controlling particle size has been precursor concentration with lower concentrations leading to smaller particle sizes. Perhaps this is not so surprising since precursor concentration will have little effect on other properties as long as it is low enough to not impact the plasma. Nonetheless, in the future, better insight into the coupled effects could enable even better control over particle properties.

**Compositional Control in Alloyed NPs:** Extending from size control, compositional control in alloyed NPs made up of more than one metal has been demonstrated by varying the ratio of the respective vapor precursors. Correlations have been found between the ratio of the precursor vapors and the relative amount of the metals in the as-grown NPs. The assumption is that the different precursors dissociate similarly to produce the necessary radicals for particle nucleation. Refinements in experiments and modeling will be able to validate such an assumption and, if relevant, provide corrections that could lead to improved control over the precise particle composition. While other compositional control such as core-shell architectures are desired, to our knowledge, have not yet been reported. A potential strategy would be to operate microplasmas in series with the precursor vapors introduced sequentially. A key challenge will be controlling nucleation versus deposition on the pre-existing NPs in the second reactor.

**NP Shaping:** The shapes of NPs and NSs determine their properties. Consequently, shape control is important in the NP and NS synthesis. In general, during a typical chemical synthesis of NPs, low-index facets and spherical and spherical-like shapes are preferentially formed under thermodynamically controlled conditions while high-index facets and irregular shapes tend to be formed under kinetically controlled conditions. Therefore, it is crucial to control the synthesis conditions for shape-controlled synthesis of NP. One possible way, also used in wet-chemistry, is to use surface-selective capping agents and/or ligands to control the shapes. Recently, it has been reported that NP shapes can be affected by the process conditions in the microplasma synthesis. In gas-phase microplasma synthesis, it is noted that the shapes of the Sn NPs can be affected by the gas flow rates.<sup>[26]</sup> Some other factors that may affect NP properties and production rates include the gas flow that may affect the energy exchange between microplasmas, electromagnetic fields, precursors, and radiation

fluxes. Another possible effect is related to inhomogeneous gas flows which may increase turbulence and cooling or enhance precursor mixing. However, similar to chemical microreactors, small flow volumes in microplasmas likely facilitate effective precursor mixing without inducing significant turbulence and instabilities in the gas flow.

According to the high-resolution TEM (HRTEM) microanalysis, the as-synthesized Sn NPs prepared with a gas flow rate of 1 sLm featured highly spherical shapes while the one prepared with gas flow rate of 0.25 sLm presented slightly elongated shapes. The gas phase chemistry and other microplasma features (e.g., precursor delivery, reactor geometry/configuration, etc.) may also play a role in controlling the particle shape. It is demonstrated that cubic-shaped TiN NPs with (200) facet were synthesized in a gas-phase microplasma with titanium tetrachloride (TiCl<sub>4</sub>) as precursor and nitrogen gas as the reactant<sup>[116]</sup> while TiN NPs showed spherical-like shapes using tetrakis(dimethylamino) titanium and ammonia as the precursors.<sup>[117]</sup> On the other hand, in the liquid-phase microplasma synthesis, the shapes of In<sub>2</sub>O<sub>3</sub> NPs were controlled by the reaction time. The NP shape can be transformed from spherical particles at short reaction times (10 min), to rods at middle reaction times (15 min), to sheets at long reaction times (70 min), and even to cubes at very long reaction times (240 min).<sup>[69]</sup> The shapes of ZnO NSs have been controlled by varying the capping agents during the microplasma-assisted liquid-phase synthesis.<sup>[78,79]</sup> It is interesting to observe that nanosheets, nanodrums, and nanoneedles of ZnO NSs can be produced by using sodium dodecyl sulfate, fructose, and cetrimonium bromide, respectively, during the microplasma-assisted synthesis at room temperature, similar to wet chemical approaches.

**Nitrogen Breakdown for Nitride Materials:** Dissociation of N<sub>2</sub> molecule containing a triple nitrogen bond, is very energy demanding. Microplasmas effectively overcome this problem and facilitate the formation of nitride-based NSs including titanium nitride (TiN) NPs<sup>[116,117]</sup> and aluminum nitride (AlN) NPs<sup>[118]</sup> from suitable precursors. Interestingly, emerging materials such as low-dielectric constant (low-k) zeolites thin films composed with zeolite particles with uniform size distribution and high crystallinity can be fabricated by nitrogen microplasmas at ambient pressure.<sup>[119]</sup>

**Single-Step Processes:** It is also possible to perform materials synthesis and patterning on substrates in a single step by using microplasma-based process. It not only overcomes the problem of multiple-step materials processing required in conventional methods but also potentially can be applied for large-scale and continuous process, e.g., roll-to-roll or additive manufacturing.

**Compatibility with Printing Technologies:** It has been recently shown that GO films can be directly printed on substrates and simultaneously be reduced using an atmospheric pressure plasma jet.<sup>[120]</sup> The microplasma-based jets can also be used to perform maskless etching of graphene for flexible micro-supercapacitor fabrication at ambient pressure.<sup>[121]</sup>

**Surface Modifications at Ambient Conditions:** The high energy electrons, radicals, and reactive species generated in the microplasma can be used for surface modification of materials. It has been reported that the surface properties of CNMs,<sup>[122,123]</sup> polymeric films,<sup>[124–128]</sup> can be modified by microplasmas-based

treatments. The plasma modification step can further change the optical, electronic, and other properties of materials. Interestingly, some of the microplasma features discussed in this section, are also useful in the selected industry-oriented applications including reactive liquid media for sterilization and plasma discharges for high-performance commercial lighting, water purification, and other systems, presented in the following section.

## 4. Microplasma Devices and Applications

As discussed in Section 2, microplasmas represent active chemical and electromagnetic media which makes them of considerable value in the fabrication and analysis of advanced materials and devices, but also as synthetic materials whose properties are dynamic. To illustrate the potential utility of microplasmas, we present here selected microplasma devices that are most relevant to the electronics and photonics materials communities. Several of these have been commercialized over the past decade (and are currently being manufactured) and the applications described include: i) chemically reactive media for solid and liquid materials processing; ii) advanced vacuum ultraviolet (VUV)/UV (“light”) sources for materials analysis and processing; and iii) dynamic electromagnetic media for artificial, 3D crystals and metamaterials.

### 4.1. Chemically Active Media for Solid and Liquid Materials Processing

The unique properties of microplasmas discussed in Section 2 provide the opportunity to alter the chemistry and physics of gas/solid interfaces so as to selectively generate reactive species. The geometry, materials, operating pressure, background gas, and driving voltage waveform for microplasma devices are the primary factors determining the reduced electric field strength ( $E/N$ , where  $E$  and  $N$  are the electric field strength and background gas number density, respectively) at any point in the plasma. This important parameter dictates the inelastic collision rates in the plasma and, most importantly, the resulting reaction products.

**Materials Etching and Synthesis:** The earliest report of Si etching<sup>[129]</sup> by a DC microdischarge formed in Ar/CF<sub>4</sub> gas mixtures demonstrated etching rates up to 7 μm min<sup>-1</sup>. In this process, Ar ion bombardment of the surface, and discharge current densities of ≈30 mA cm<sup>-2</sup>, were responsible for the rapid formation of bowl-shaped cavities in the Si cathode. More recently, Si etching using RF-powered plasma jets with diameters as small as 500 μm was reported.<sup>[130]</sup> In these studies, He/N<sub>2</sub>/CF<sub>4</sub> mixtures served as the feedstock gas for the plasma, and etching efficiencies (Si atoms removed per incident fluorine atom) of 15% were observed. With respect to other substrate materials, it was demonstrated<sup>[131]</sup> that the structure of polymer films could be altered in a controllable and spatially selective manner through exposure to microplasmas. The impact of microplasmas on polymer surfaces was later exploited to pattern biomolecules (streptavidin) on polyethylene oxide.<sup>[132]</sup> For electronics applications, linear arrays of plasma jets<sup>[85,86]</sup> have

been designed and characterized, and subsequently applied for etching of a photoresist with spatial resolutions in the 250–400  $\mu\text{m}$  range.

Arrays of microplasmas can be conveniently generated within microchemical reactors, and several microplasma systems have been commercialized. For example, low-cost, disposable microreactors were fabricated in a polymer by replica molding and applied to the spatially localized deposition of sulfur.<sup>[133]</sup> Carbon disulfide ( $\text{CS}_2$ ) was dissociated in  $10 \times 10$  arrays of 400  $\mu\text{m}$  diameter microcavities by microplasmas generated in an Ar flow at atmospheric pressure. Sulfur was deposited in the downstream portion of the reactor, which served as a flowing afterglow plasma. The morphology and composition of the deposit suggested that the growth process occurs by heterogeneous reactions and that the scission of at least one  $\text{CS}_2$  bond is energetically efficient. We wish to emphasize the generality of this deposition process in which energy stored in ionized (or excited) states of Ar or the argon dimer ( $\text{Ar}_2$ ) can be transferred to the acceptor molecule ( $\text{CS}_2$ ) which culminates in the growth of a film or the deposition of a bulk solid. Similar processes appear to be feasible for the Group III and Group V elements at the heart of electronic and photonic devices. Subsequent advances were made in the development and applications of various types of microplasma-based chemical processing reactors.<sup>[134,135]</sup> Importantly, the synergy of microplasma and microfluidic technologies offers great potential for the development of next generation, materials synthesis reactors offering the advantages of atmospheric pressure operation and temperatures as low as 300–350 K, without the need for catalysts.

*Materials Processing with Microplasma-Generated Excited Species:* Microplasmas are efficient generators of excited reactive species that can be tailored for diverse applications in the treatment of both solid and liquid materials. One striking example of a recently commercialized microplasma reactor process is the production of ozone ( $\text{O}_3$ ) for the disinfection of drinking water and the treatment of industrial or municipal wastewater (“gray water”).<sup>[136]</sup> These reactors are also suitable for diverse surface modifications, such as imparting hydrophilic surface properties to soft polymeric or carbon-based materials and conditioning of dental implant materials. Commercially available, modular ozone-generating systems based on assemblies of microchannel plasma “chips,” fabricated in nanoporous alumina ( $\text{Al}_2\text{O}_3$ ), are capable of producing ozone with an electrical efficiency above  $120 \text{ g kWh}^{-1}$ .<sup>[136]</sup> **Figure 7a** is a photograph of a commercial microplasma ozone module comprising four chips which can be connected in tandem or in parallel for the purpose of increasing the ozone concentration or the ozone production rate, respectively.

This device is a salient example of a synergistic interaction between a microplasma and an advanced nanomaterial. Indeed, the performance of the chips at the heart of these systems hinges on the structure of the nanoporous alumina that serves as a dielectric barrier film isolating the plasma from the electrode. Comprising close-packed arrays of 40–120 nm hexagonal pores, the alumina films are characterized by dielectric breakdown strengths more than double that for bulk alumina. As a result, the dielectric film thicknesses can be reduced relative to those required for other suitable materials, thereby elevating the electrical efficiency for the reactor. Furthermore, this

microreactor technology has been scaled in ozone generation by combining the outputs of multiple modules. Engineering tests with as many as 18 modules have demonstrated that the ozone production rate (expressed in grams per hour) scales linearly with the number of modules up to at least  $100 \text{ g h}^{-1}$ .<sup>[136]</sup> **Figure 7b** is an optical microscopy image of a 48-channel reactor, operating in one atmosphere of pure oxygen that is flowing at a volumetric rate of 2 slm.<sup>[137]</sup>

In contrast to conventional ozone generators, the microplasma-based ozone systems of **Figure 7** are compact and capable of operating with humid air as the feedstock gas. A single chip produces 0.3 g of ozone per hour with room air, and the power consumption of this one-chip reactor is 12 W. Although the ozone output of one chip is modest, it is more than sufficient for disinfecting the water required daily by a single family. Consequently, the low power requirements and cost of this technology have resulted in microplasma ozone systems being in operation currently in more than 35 countries worldwide. Many systems are located in off-the-grid, solar-powered settings, and **Figure 7c** is a photograph of a small ozone system disinfecting water for a hospital in Jos, Nigeria that is situated outside a refugee camp. Previously, water suitable for surgery, wound irrigation, and other medical treatments was severely limited in both quality and quantity because of the expense and difficulty of transporting traditional chemical disinfectants (such as sodium hypochlorite), on a periodic basis, to remote locations. Powered by a 15 W solar panel, systems such as that of **Figure 7c** are also disinfecting drinking water within the refugee camp, and elsewhere in Africa and other countries.

Commercial applications into which this technology has already made significant inroads include the cold storage of fruits and vegetables (see **Figure 7d**), the disinfection of industrial and farm wastewater, and the treatment of water for pools and saunas. **Figure 7d** presents two photographs of tangerines in a large cold storage facility in South Korea in which the lifetime of vegetables and fruit is extended by exposure to low levels of microplasma-generated ozone. The fruit shown in the upper photograph has been stored in the facility in room air having a low ozone concentration, whereas the tangerines in the lower photograph were stored for the same length of time and at the same temperature but in the absence of ozone. Serving as a control, the tangerines in the bottom image have noticeably deteriorated. Similar extensions of fruit and vegetable storage times have been realized for avocados in Chile.

The particular applications of microplasma technology presented in **Figure 7** are a vivid evidence of its ability to meet demanding humanitarian, industrial, and consumer requirements because the unique properties of microplasma arrays yield reduced power consumption, cost, and volume. The resiliency and efficiency of microplasma ozone technology in humid, high temperature environments, specifically, are at least partially attributable to the extraordinary breakdown strength and porosity of nanoporous alumina.

Another promising application of microplasma reactor technology in materials processing is that of printing. A combined printing and ALD system is based on the decomposition of volatile precursors at a surface with microplasmas generated within capillaries.<sup>[91]</sup> Spatial resolution as low as 200  $\mu\text{m}$  and

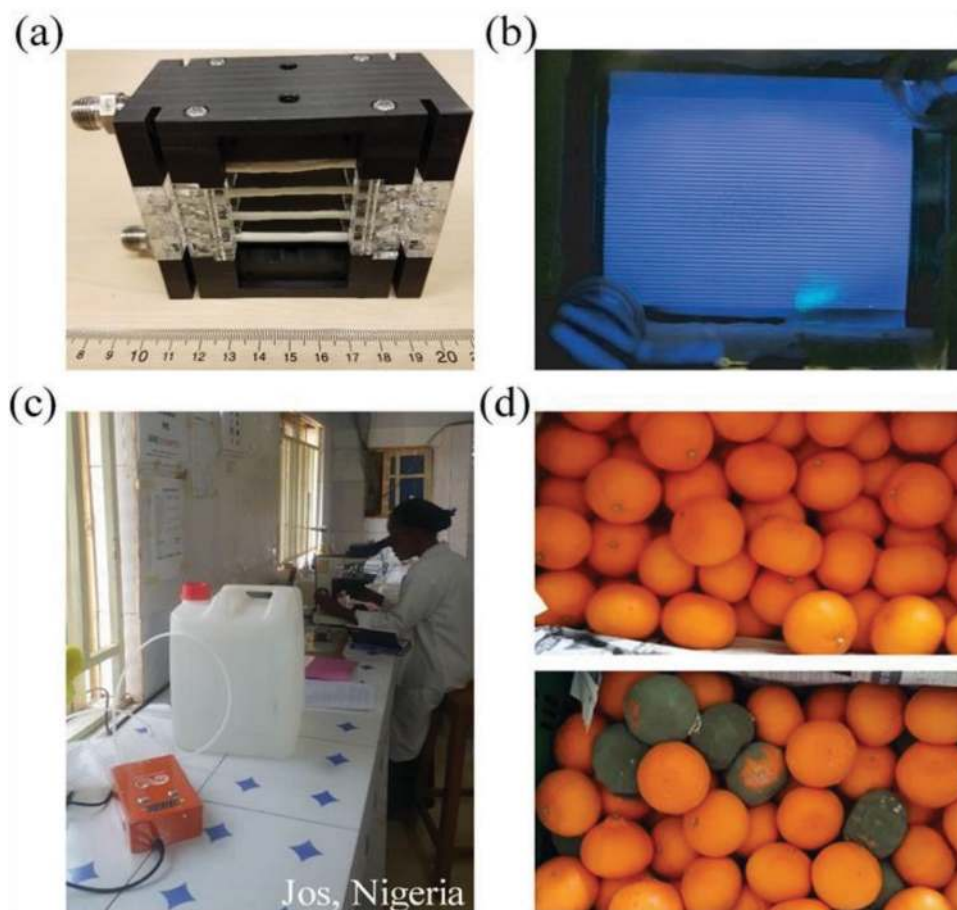


**Figure 7.** Real-world applications of microplasmas. a) Photograph of a commercial module comprising four Al/Al<sub>2</sub>O<sub>3</sub> “chips,” and capable of producing more than 6 g of ozone per hour. Photograph provided by and reproduced with permission from EP Purification, Inc. b) Optical microscopy image (photographed in plan view through a glass window) of a 48 channel microreactor in which ozone is generated in the microchannel plasmas. Reproduced with permission.<sup>[137]</sup> Copyright 2013, Institute of Physics. c) Photograph of a small EP Purification system providing disinfected surgical water for a small hospital outside a refugee camp in Jos, Nigeria. Photo provided by and reproduced with permission from EP Purification). d) Photographs of tangerines in a cold storage facility in South Korea. The fruit in the upper panel has been exposed to low concentrations of ozone (produced by a system similar to that of (c)) in the facility. The lower photograph shows tangerines stored for the same period of time and at the same temperature, but in the absence of ozone. Top photograph provided by and used with permission from Ozonaid (Seoul, South Korea). Bottom photograph provided by and reproduced with permission from EP Purification.

printing speeds up to  $0.2 \text{ cm}^2 \text{ s}^{-1}$  are currently available with these commercial systems.

#### 4.2. Advanced Light Sources for Materials Analysis and Photochemistry

Microplasmas are efficient emitters in the UV and VUV spectral regions. Research of the past two decades into the spectral and electrical properties of microplasma arrays recently culminated in the demonstration of flat lamps generating more than 25 W of average power at 172 nm from the Xe<sub>2</sub> molecule in the VUV region.<sup>[138]</sup> Capable of realizing intensities greater than  $300 \text{ mW cm}^{-2}$  at pulse repetition frequencies above 130 kHz, these lamps comprise two interlaced arrays of microcavities and offer active areas of  $\approx 90 \text{ cm}^2$ , a spectral bandwidth of roughly 9 nm, and peak (instantaneous) intensities above 600 W. The reported intensity and average power for these lamps are unprecedented in the VUV spectral region (wavelengths of

100–200 nm) which has been dominated by low power lamps for more than a century. To put these lamp parameters into perspective, the steady-state intensity currently produced by microcavity plasma lamps in the  $172 \pm 5 \text{ nm}$  interval is the same as that generated by a blackbody emitter having a radiation temperature of 16 500 K. One such emitter is the B3 class star Eta Ursae Major located in the main sequence of the Cygnus constellation. Another way to assess such extraordinary intensities in the VUV region is to recognize that the fluence (expressed in  $\text{J cm}^{-2}$ ) received from a 1 min exposure to a 172 nm intensity of  $100 \text{ mW cm}^{-2}$  is equivalent to 2 years of solar exposure immediately outside the Earth’s atmosphere.

The motivation for offering the above comparisons is that the intensities now available from thin (less than 6 mm in thickness) and efficient, microplasma-driven lamps are poised to revolutionize the photochemical processing and spectroscopic analysis of materials. Lamps of design similar to that of the 172 nm emitters have also been realized at 147, 222, 240–260, and 308 nm, which adds versatility to this new class

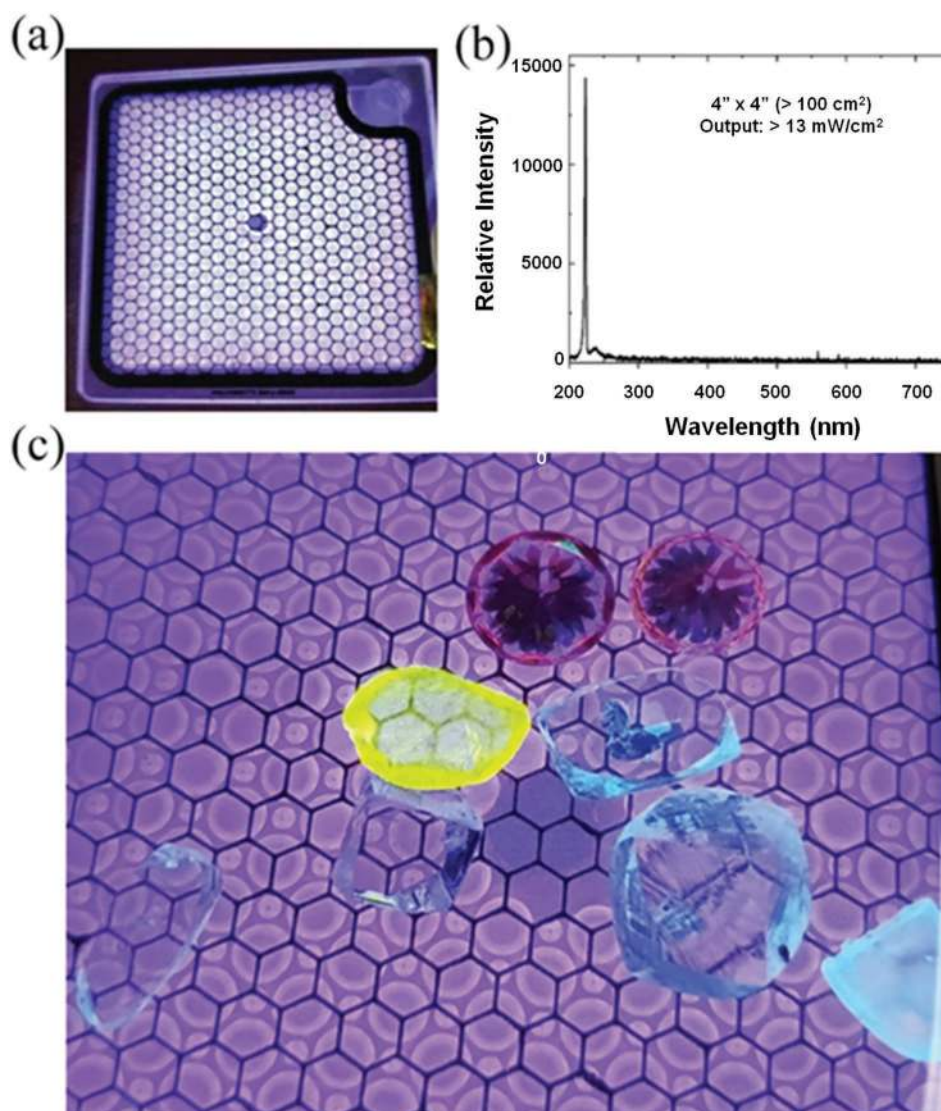


**Figure 8.** Microplasma applications in lighting devices and materials analysis. a) Photograph of a 5 cm × 5 cm lamp emitting radiation from the KrCl molecule. b) Spectrum of the lamp in (a), consisting of a single peak at 222 nm, and a weak wing extending to longer wavelengths. c) Photograph in plan view of an assortment of natural and synthetic diamonds lying on the surface of a 222 nm emitting microplasma array lamp. Natural diamonds emit only soft blue light—all others are synthetic. Photographs and spectrum provided by and reproduced with permission of Eden Park Illumination.

of lamps in several emerging applications. As one example, **Figure 8a** presents a photograph of a 5 × 5 cm<sup>2</sup> (2" × 2") lamp having a rare gas/Cl<sub>2</sub> mixture. As shown in **Figure 8b**, the lamp generates a single narrow peak at 222 nm that is emitted by the KrCl molecule. Commercial applications of lamps operating at this wavelength include materials analysis and photochemistry.

A promising, commercialized application of 222 nm emitting lamps ( $h\nu = 5.58$  eV) is that of distinguishing natural diamonds from those synthesized by CVD or high-pressure thermal processes. **Figure 8c** is a photograph of an assortment of diamonds, natural and synthetic, lying on the surface of a 222 nm microcavity plasma lamp. The weak violet emission from the lamp surface represents <2% of the total lamp power that is generated in the long-wavelength tail of the spectrum (**Figure 8b**). It is immediately obvious that each of the diamonds

fluoresces in response to the absorption of the 5.6 eV photons. Natural diamonds emit only weak blue fluorescence that decays quickly upon extinguishing the 222 nm lamp. In contrast, synthetic diamonds emit strong fluorescence in a variety of colors (such as yellow and deep red in **Figure 8c**), depending on the process by which the diamonds were grown. In most instances, the fluorescence emanates from color centers and other optically active defects in the crystal. Although this UV-excited fluorescence mechanism is straightforward, it has proven to be of considerable value to the diamond industry. As of the date of this paper submission, more than 1000 automated diamond identification systems have been manufactured for jewelers and diamond distributors.

The applications available to the 7.2 eV photons produced by Xe<sub>2</sub>-emitting lamps ( $\lambda = 172$  nm) mentioned earlier appear to be quite broad, particularly insofar as materials processing



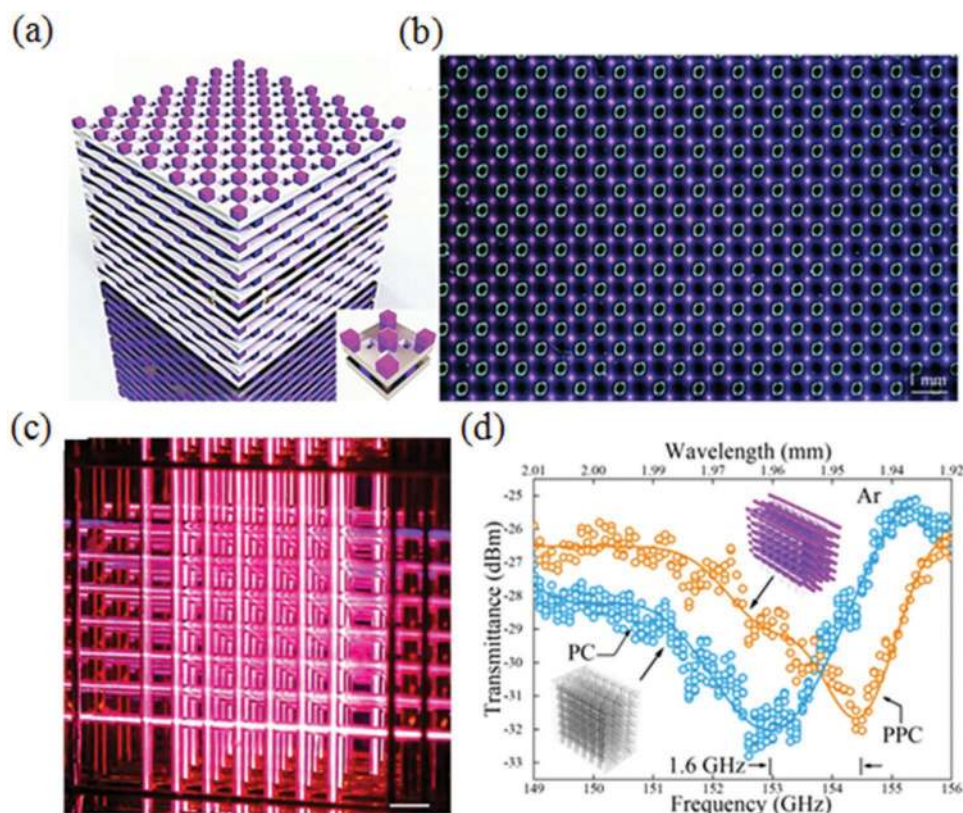


**Figure 9.** Microplasma-materials synergy: active electromagnetic devices. a) Isometric projection of a 3D polymer scaffold designed and tested for the generation of large, spatially periodic microplasma arrays. b) When filled with argon, this structure produces plasma arrays having a cubic structure as shown by the plan view optical microscopy image at right. In this image, the square polymer posts are being viewed head-on and are identifiable by a blue-green perimeter. c) Optical image of a 3D PPC operating in  $\approx 1$  atm of helium. d) Transmission spectra in the 149–156 GHz interval for the scaffold of an eight-layer PPC (blue trace) and the same crystal with Ar microplasmas generated in layers No. 2, 4, 6, and 8 of the crystal (orange curve). Illustrations and optical microscopy images. Reproduced under the terms of the CC-BY Creative Commons Creative license (<http://creativecommons.org/licenses/by/4.0/>).<sup>[142]</sup> Copyright 2019, The Authors, published by AIP Publishing.

is concerned. For example, 172 nm radiation is capable of patterning polymer surfaces as a result of the photodissociation and ablation of hydrocarbon materials.<sup>[139]</sup> Other applications of the 172–308 nm lamps described above include photo-processing in the gas and solid phases, nanofabrication, structural modifications to solid/solid, liquid, or gas interfaces, and water purification.<sup>[140]</sup>

#### 4.3. Active Electromagnetic Media for Artificial 3D Optical Metamaterials

One of the achievements of microplasma technology of the past decade is the ability to assemble artificial geometric structures comprising microplasma elements such as microcolumns, disks, and even cubes. Because spatially periodic, plasma-dielectric arrays, in particular, are synthetic materials whose properties can be altered at electronic speeds, new opportunities for electromagnetic applications are now accessible. To that end, the transmission spectrum of 2D microplasma jet arrays in which the plasma columns have a pitch of 1.0 mm, was measured.<sup>[141]</sup> Consequently, the Bragg frequency of each row of jets is 150 GHz, and experiments probing the array (in the plane orthogonal to the axes of the plasma jets) revealed the existence of a weak attenuation resonance at roughly 157 GHz.

**Figure 9** shows an example of a multilayer microplasma device in which each layer is 3D-printed.<sup>[142]</sup> Figure 9a is an illustration (in isometric projection) of the structure in which the pink regions represent polymer posts that serve the dual function of separating adjacent layers of the periodic structure and defining the geometry of the microplasmas constituting the 3D array. When filled with the desired gas, or gas mixture, and powered by a voltage applied to planar indium tin oxide electrodes on opposing faces of the structure, the scaffold of Figure 9a becomes a cubic network of microplasmas that can be designed for specific applications. Figure 9b is an optical microscopy image, recorded along an axis orthogonal to the surface plane of the structure (i.e., plan view), of the cubic plasma network generated within the structure of Figure 9a when Ar gas (pressure  $\approx 1$  atm) is introduced.

Although the 3D network of Figure 9a,b is an interesting artificial plasma structure, it does not allow for reconfigurability. Because the scaffold is a solid and the microplasmas are not individually addressable, the entire structure is static and, therefore, not tunable. To correct this shortcoming, both 2D and 3D arrays of microplasma columns have been demonstrated, and Figure 9c is a microphotograph of a 3D plasma photonic crystal (PPC) having a woodpile structure and operating in 1 atm of helium.<sup>[142]</sup> This array comprises 355  $\mu\text{m}$  diameter microplasmas generated within cylindrical channels

formed in a poly(dimethylsiloxane) (PDMS) block (scaffold) by replica molding, and each layer of the crystal is a planar Bragg grating having a columnar plasma pitch of 1.0 mm. Adjacent planes can be spaced by 0.5–1.0 mm with a positional accuracy of 10  $\mu\text{m}$ . After the PDMS scaffold containing the arrays of microchannels is completed, electrodes are inserted into both ends of every channel which are filled with the desired gas.

The result of this fabrication procedure, developed over a period of several years, is a series of photonic crystals (such as that of Figure 9c) that can be rapidly reconfigured at will, and designed to serve as phase shifters, filters, and resonators in the microwave, mm-wave, and THz spectral regions. Because the dielectric permittivity of low-temperature plasma is dependent upon both the electron density and collision frequency for momentum transfer of the plasma, these photonic crystals are tunable with predetermined spectral characteristics. Scores of such PPCs have been fabricated and tested in the 120–350 GHz frequency interval, and Figure 9d illustrates the tuning available with this PPC technology. The blue trace in Figure 9d represents the transmission spectrum for the PDMS scaffold which is itself a static photonic crystal, and the orange data points are those recorded when plasmas are ignited in layers #2, 4, 6, and 8 of an eight-layer PPC. The blue frequency shift produced by the microplasmas is 1.6 GHz.

The point to be made is that the advent of a technology for fabricating dense, 3D arrays of microplasma columns (and other geometries) with precision has enabled the realization of dynamic, functional materials based on microplasmas. These hybrid plasma/dielectric/metal materials have properties not available in the past, such as re-configurability at electronic speeds, and are ideally suited for electromagnetics applications. Therefore, the ability to electronically control the parameters of each microplasma through the applied voltage and gas/vapor mixture pressure provides access to a family of artificial advanced materials (closely related to metamaterials) of both scientific and applied interest.

## 5. Summary and Outlook

The impressive recent advances discussed above suggest that microplasmas represent a unique physicochemical environment for both fundamental studies and applications involving advanced materials. The chemical and electronic environment provided by microplasmas is strongly nonequilibrium and is capable of storing energy at densities of tens of  $\text{kW cm}^{-3}$  to  $\text{MW cm}^{-3}$ . Therefore, energy in the form of photons or charged particles can also be released efficiently by microplasmas, a property that stems from the spatial confinement of the plasma. Moreover, the nonequilibrium behavior of microplasmas results in the ability to maintain such a highly energetic state at gas temperatures that are often no more than 100–150 K above room temperature. Under such nonequilibrium and high-energy-density conditions, large concentrations of electrons, ions, radicals, and other excited, ionized and otherwise reactive species can be generated.

This exotic environment opens a range of interesting options for synthesizing or modifying a range of advanced functional nanomaterials, or otherwise use the plasma as a functional

material in its own right. Interestingly, microplasmas convert and modify matter in all four major states—namely solid, liquid, gas, and plasma. Indeed, gases are needed to generate plasmas, and plasma converts gaseous precursors into solid particles but also generates gas phase, transient molecules that efficiently emit 3.5–8 eV photons of interest for materials analysis and growth. The plasma can also interact with diverse precursors in the liquid state. Of greatest interest is the transformation of energy into matter, and vice-versa, that microplasma affords. For example, during NP synthesis, electrical energy for plasma generation is transformed into the chemical bond energies, while the electrical energy itself can be supplied by renewable (e.g., solar or wind) sources. Recalling the extraordinary number densities of electrons and the specific power loadings of the microplasma medium, it is reasonable to refer to microplasmas as a nonequilibrium, energy-matter converter.

The applications of microplasmas have been successfully demonstrated across several fields. On one hand, the microplasma synthesis of advanced functional nanomaterials (including metals, semiconductors, and oxides) with diverse morphological and structural properties opens new avenues in exploring unconventional relationships between the structure and properties of materials synthesized under nonequilibrium conditions. On the other side of the broad spectrum of applications, we have seen synergies between microplasmas and solid materials with micrometer and nanoscale dimensions leading to unconventional, dynamic-functional materials such as PPCs for active electromagnetic devices or commercial ozone generators for food and water sterilization.

These interesting features and applications suggest that research at the edge of microplasmas and advanced materials should definitely continue and expand into new areas in the years ahead. This goal can be achieved through information exchange and collaborations between researchers specializing in the fields of low-temperature plasma and materials, as well as other aligned areas. To facilitate this endeavor, we discuss below a few selected areas where we see opportunities and research needs for both fundamental studies and industry-oriented applications.

One important area of research is to elucidate the multiple roles of the microplasma in the synthesis of nanomaterials, leading to the materials properties desired for specific applications. This type of scientific enquiry is common in the plasma nanoscience research field, where various low-temperature plasmas have been shown to enable the synthesis or processing of materials rather than merely assisting baseline thermal or chemical processes.<sup>[143]</sup> Many microplasma-based processes exhibit dramatic changes when plasma is introduced, e.g., those processes for which the formation of a material does not even proceed without plasma excitation.

For better understanding of these processes, numerical modeling and simulation appear indispensable. The obvious complexity in this regard is associated with the multimodal features of microplasmas that play a critical role in nanomaterials synthesis and processing. Therefore, it is imperative to be able to quantify and discriminate between the effects of different reactive plasma agents (such as electrons, ions, radicals, excited molecules, light, heat, etc.) on the resulting morphology (e.g., shapes), sizes, chemical structure,

and functionalization of the resulting nanomaterials or, alternatively, on the specific performance indicators (e.g., flux of reactive species or electromagnetic radiation) of the microplasma-based devices.

To this end, it is important to apply the advanced theoretical concepts and models related to energy transfer from the initially excited electrons to the atoms or molecules of the operating gas, and relate any specific redistribution of the input energy to the desired practical outcomes in terms of materials synthesis or other applications of microplasmas discussed above. A practical way to implement this complex task is by applying new theoretical concepts such as “The Energy Tree” which can be used to describe the partitioning of the initial electric energy input among the possible energy exit channels in plasma discharges.<sup>[144]</sup> The outcomes will certainly depend on the specific process, type, and parameters of the applied voltage, and the operating gases or gas mixtures. For example, if the synthesis of carbon NPs (e.g., GQDs) from greenhouse gas precursors (e.g., CO<sub>2</sub> or CH<sub>4</sub>) is concerned, the first step is to model the extraction of carbon atoms from the source molecules, followed by the particle formation and shaping. Advanced models of carbon species production, nucleation of small NPs, and shape formation (e.g., through faceting) that account for the effects of microscale confinement and the associated effects of the boundaries that limit the microplasmas, are needed. These models mostly exist for other atmospheric pressure plasmas, e.g., for larger-scale plasma jets or dielectric barrier discharges.<sup>[145]</sup> Importantly, these models require significant improvements because of the complexities related not only with the limited microscopic space, but also with the prevailing nonequilibrium effects discussed in Section 2. The lack of equilibration among the plasma species would lead to the need to customize the energy distribution functions for both electrons and ions, which in turn would affect the rates of most of the elementary reactions involved in the (e.g., collision-dominated) production and nucleation of the building species for the NP production. The presence of strong electric fields even at modest applied voltages in confined microspaces is expected to significantly affect the nucleation, growth, and shaping of NPs, leading to the possibly stronger ion- and polarization-related effects than in other types of plasmas. The ion impacts on the particle surface would definitely require advanced numerical modeling of the microplasma-surface interactions, again, within microscopic space.

As discussed in Section 4, applications of microplasmas in sterilization and light sources require improved models of the production of relevant reactive agents. Specifically, for sterilization applications, highly selective production of ozone species is required. As mentioned in Section 4, the mechanism of the highly selective ozone output from the microcavity plasma devices is intimately related to the sizes of the cavities where the plasmas are generated, and, even more importantly, to the sizes (e.g., diameters and lengths) of the nanoscale channels in anodic aluminum oxide membranes that are used to selectively pass the ozone species. These models presently do not exist and offer obvious opportunities for the development of the new advanced models of reactive species generation in microplasmas and transport through nanochannels. On the other hand, although the new models of microplasmas as active

electromagnetic sources can be built on the existing models of radiation processes in atmospheric pressure plasmas, they would require rigorous account of the regular microscopic features of the devices, e.g., of the 3D light-emitting stacks depicted in Figure 9b. Studies of possible benefits of the microplasma-associated photochemistry on nanomaterials production represent another interesting opportunity.

With the advent of radically new concepts and approaches to describing and quantifying elementary processes on plasma-solid surfaces, at atomic-to-microscales such as the “plasma interface,”<sup>[146]</sup> there is a clear need to apply these and other concepts and methods to better understand and control microplasma–NP interactions, ideally from the moment of initial nuclei formation. The ability to describe specific phase formation and extend this description to multi-material, multi-phase systems, represents a significant challenge.

The above points arose primarily because of the recognized ability of microplasmas to:

- Accelerate chemical reactions and nucleation;
- Synthesize a broad range of nonequilibrium, metastable materials,

both stemming from the high-energy-density and non-equilibrium properties of microplasmas. Consequently, microplasma-based processes should particularly suit practical applications for which the deposition of electrical and optical power into small volumes while maintaining sub-500 K temperatures is critical. Examples of applications on which we envision microplasma research to have a steadily rising impact are:

- Integration of microplasmas with plasma printing, to diversify and improve the existing platforms in the quality and multiscale (from atomic-to-microscale) structuring of printed patterns, and improving linewidth resolution where possible;
- Application of microplasma-produced NPs (e.g., jetting, printing, spraying, deposition) onto a broad range of materials, at desirable rates and surface temperatures. This ability requires improvements in the presently available ability to control NP sizes and compositions. However, it can also be regarded as another means to engage with advanced digital manufacturing technologies (e.g., robotics, 3D processing, etc.) beyond conventional plasma printing;
- Multiple opportunities exist in the production of ultrasmall NPs made of difficult to mix, or even immiscible, materials. Current state-of-the art using diverse (e.g., organometallic, inorganometallic, metal salts, etc.) precursor chemistries and post-processing (surface functionalization, thermal annealing, etc.) allows synthesis of such particles comprising a large number (e.g., up to seven) of elements and with controlled grain/domain separation, alloying, core–shell structures, etc.<sup>[147,148]</sup> A clear opportunity for microplasmas lies in the need to drastically accelerate these processes, with the goal of surpassing existing processes in terms of productivity and precision.
- Combining microplasmas with microreactor technologies offers an exceptional opportunity to massively parallelize

chemical processes in small reactor channels with micrometer dimensions. In this way, one could potentially realize very large, scalable arrays of microplasmas capable of performing diverse functions, ranging from waste (e.g., CO<sub>2</sub>) conversion to precise and energy-efficient synthesis of advanced materials and fuels of interest to the energy, chemical, telecom, construction, and optical systems industries.

- Further enhancements can be achieved if plasma jet arrays synergistically interact with precursors directly placed on the surface and the surface itself acts as a catalyst. This multiscale plasma-catalytic on-surface assembly<sup>[149]</sup> relies on combinatorial plasma nanotechnology and plasma catalysis effects. This approach may be of interest as a promising future manufacturing platform which combines the benefits of plasma-assisted control at atomic to microscales and scalability to large processing areas on one hand and digital prototyping and process automation on the other one.
- Widespread use of ultrahigh-power microplasma-array light sources (e.g., UV/VUV) for materials synthesis and processing, which is critical to new photochemistry approaches to synthesizing previously inaccessible soft materials. An example is that of degradable plastics produced by targeted bond engineering and photoinduced “click chemistry.”<sup>[150]</sup> These materials may lead to a new generation of plastic materials that pose no contamination hazard to our planet.
- As mentioned earlier, better use of renewable (e.g., solar and wind) energy for microplasma generation, and scaling the discharges by employing integrated electrode arrays may be a promising approach to developing zero-emissions energy conversion systems that are readily transported and operated off-the-grid. A potential impact of integrating with renewable energy is the possibility of sustainably converting cheap feedstocks such as CO<sub>2</sub>, water, and N<sub>2</sub> to value-added chemicals.<sup>[151,152]</sup>

The above list of opportunities for future microplasma-focused research and development is certainly not exhaustive, and one should expect many more exciting discoveries and applications to arise in the coming years. Importantly, numerous synergies at the cutting edge between research in low-temperature plasmas and advanced materials will enrich both fields while accelerating the translation of new discoveries into commercial applications.

## Acknowledgements

The authors greatly appreciate the efforts of all researchers who have worked in any of the relevant areas and apologize if any of contributions were not included due to specific focus and size limits of this article. W.-H.C. acknowledges the support of the Ministry of Science and Technology (MOST) of Taiwan (under grant no. MOST 107-2628-E-011-002-MY3). D.M. acknowledges the support of EPSRC funding through EP/M024938/1, EP/M015211/1, EP/R023638/1, and EP/R008841/1. R.M.S. acknowledges the support of the Department of Energy under grant no. DE-SC0018202. J.G.E. thanks P. P. Sun, J. H. Cho, S.-J. Park, and C. M. Herring for valuable discussions, and acknowledges the support of the U.S. Air Force Office of Scientific Research under grant no. FA9550-14-1-0002. K.O. thanks the Australian Research Council for partial support.

## Conflict of Interest

The authors declare no conflict of interest.

## Keywords

materials and devices, microplasmas, nanomaterials, nanoscale synthesis

Received: August 24, 2019

Revised: September 28, 2019

Published online:

- [1] A. P. Alivisatos, *Science* **1996**, 271, 933.
- [2] E. Roduner, *Chem. Soc. Rev.* **2006**, 35, 583.
- [3] a) F. Guinea, M. I. Katsnelson, A. K. Geim, *Nat. Phys.* **2010**, 6, 30; b) S. Marre, J. Park, J. Rempel, J. Guan, M. G. Bawendi, K. F. Jensen, *Adv. Mater.* **2008**, 20, 4830.
- [4] a) B. Ni, Y. Shi, X. Wang, *Adv. Mater.* **2018**, 30, 1802031; b) M. Bruchez, M. Moronne, P. Gin, S. Weiss, A. P. Alivisatos, *Science* **1998**, 281, 1533; c) V. Porto, E. Borrajo, D. Buceta, C. Carneiro, S. Huseyinova, B. Dominguez, K. J. E. Borgman, M. Lakadamyali, M. F. Garcia-Parajo, J. Neissa, T. Garcia-Caballero, G. Barone, M. C. Blanco, N. Busto, B. Garcia, J. M. Leal, J. Blanco, J. Rivas, M. A. Lopez-Quintela, F. Dominguez, *Adv. Mater.* **2018**, 30, 1801317; d) J. Zhang, X. Hao, N. Rowell, T. Kreouzis, S. Han, H. Fan, C. Zhang, C. Hu, M. Zhang, K. Yu, *J. Phys. Chem. Lett.* **2018**, 9, 3660; e) X.-B. Han, X.-Y. Tang, Y. Lin, E. Gracia-Espino, S.-G. Liu, H.-W. Liang, G.-Z. Hu, X.-J. Zhao, H.-G. Liao, Y.-Z. Tan, T. Wagberg, S.-Y. Xie, L.-S. Zheng, *J. Am. Chem. Soc.* **2019**, 141, 232; f) J. Wang, C. F. Mbah, T. Przybilla, B. A. Zubiri, E. Spiecker, M. Engel, N. Vogel, *Nat. Commun.* **2018**, 9, 5259.
- [5] a) N. Wang, Q. Sun, J. Yu, *Adv. Mater.* **2019**, 31, 1803966; b) R. Lv, P. Yang, B. Hu, J. Xu, W. Shang, J. Tian, *ACS Nano* **2017**, 11, 1064.
- [6] a) I. Adamovich, S. D. Baalrud, A. Bogaerts, P. J. Bruggeman, M. Cappelli, V. Colombo, U. Czarnetzki, U. Ebert, J. G. Eden, P. Favia, D. B. Graves, S. Hamaguchi, G. Hieftje, M. Hori, I. D. Kaganovich, U. Kortshagen, M. J. Kushner, N. J. Mason, S. Mazouffre, S. Mededovic Thagard, H.-R. Metelmann, A. Mizuno, E. Moreau, A. B. Murphy, B. A. Niemira, G. S. Oehrlein, Z. Lj Petrovic, L. C. Pitchford, Y.-K. Pu, S. Rauf, O. Sakai, S. Samukawa, S. Starikovskaia, J. Tennyson, K. Terashima, M. M. Turner, M. C. M. van de Sanden, A. Vardelle, *J. Phys. D: Appl. Phys.* **2017**, 50, 32300; b) U. Kortshagen, R. M. Sankaran, R. N. Pereira, S. L. Girshick, J. J. Wu, E. S. Aydil, *Chem. Rev.* **2016**, 116, 11061; c) G. Saito, T. Akiyama, *J. Nanomater.* **2015**, 115, 123696; d) Q. Chen, J. Li, Y. Li, *J. Phys. D: Appl. Phys.* **2015**, 48, 424005; e) K. Tachibana, *IEEJ Trans. Electr. Electron. Eng.* **2006**, 1, 145; f) K. H. Schoenbach, K. Becker, *Eur. Phys. J. D* **2016**, 70, 29; g) D. Mariotti, R. M. Sankaran, *J. Phys. D: Appl. Phys.* **2010**, 43, 323001; h) D. Mariotti, R. M. Sankaran, *J. Phys. D: Appl. Phys.* **2011**, 44, 174023; i) S. Dou, L. Tao, R. Wang, S. E. Hankari, R. Chen, S. Wang, *Adv. Mater.* **2018**, 30, 1705850.
- [7] a) K. H. Becker, K. H. Schoenbach, J. G. Eden, *J. Phys. D: Appl. Phys.* **2006**, 39, R55; b) L. Lin, Q. Wang, *Plasma Chem. Plasma Process.* **2015**, 35, 925; c) D. Mariotti, K. Ostrikov, *J. Phys. D: Appl. Phys.* **2009**, 42, 092002.
- [8] A. Wagner, D. Mariotti, K. J. Yurchenko, T. K. Das, *Phys. Rev. E* **2009**, 80, 065401.
- [9] a) P. J. Bruggeman, M. J. Kushner, B. R. Locke, J. G. E. Gardeniers, W. G. Graham, D. B. Graves, R. C. H. M. Hofman-Caris, D. Maric, J. P. Reid, E. Ceriani, D. Fernandez Rivas, J. E. Foster, S. C. Garrick,

- Y. Gorbanev, S. Hamaguchi, F. Iza, H. Jablonowski, E. Klimova, J. Kolb, F. Krcma, P. Lukes, Z. Machala, I. Marinov, D. Mariotti, S. Mededovic Thagard, D. Minakata, E. C. Neyts, J. Pawlat, Z. Lj Petrovic, R. Pflieger, S. Reuter, D. C. Schram, S. Schröter, M. Shiraiwa, B. Tarabová, P. A. Tsai, J. R. R. Verlet, T. von Woedtk, K. R. Wilson, K. Yasui, G. Zvereva, *Plasma Sources Sci. Technol.* **2016**, *25*, 053002; b) G. Saito, T. Akiyama, *J. Nanomater.* **2015**, *2015*, 123696; c) R. Liu, Y. Wang, D. Liu, Y. Zou, S. Wang, *Adv. Mater.* **2017**, *29*, 1701546.
- [10] C. J. Rocks, S. Mitra, M. Macias-Montero, P. Maguire, V. Svrcek, I. Levchenko, K. Ostrikov, D. Mariotti, *ACS Appl. Mater. Interfaces* **2016**, *8*, 19012.
- [11] D. Mariotti, T. Belmonte, J. Benedikt, T. Velusamy, G. Jain, V. Svrcek, *Plasma Processes Polym.* **2016**, *13*, 70.
- [12] S. Askari, I. Levchenko, K. Ostrikov, P. Maguire, D. Mariotti, *Appl. Phys. Lett.* **2014**, *104*, 163103.
- [13] N. J. Kramer, E. S. Aydil, U. R. Kortshagen, *J. Phys. D: Appl. Phys.* **2015**, *48*, 035205.
- [14] a) A. Armada-Moreira, E. Taipaleenmaki, F. Ite, Y. Zhang, B. Stadler, *Nanoscale* **2016**, *8*, 19510; b) W. Feng, E. Ueda, P. A. Levkin, *Adv. Mater.* **2018**, *30*, 1706111; c) A. Adamo, R. L. Beingsner, M. Behnam, J. Chen, T. F. Jamison, K. F. Jensen, J.-C. M. Monbaliu, A. S. Myerson, E. M. Revalor, D. R. Snead, T. Stelzer, N. Weeranoppanant, S. Y. Wong, P. Zhang, *Science* **2016**, *352*, 61; d) G. Niu, L. Zhang, A. Ruditskiy, L. Wang, Y. Xia, *Nano Lett.* **2018**, *18*, 3879.
- [15] Maguire, D. Rutherford, M. Macias-Montero, C. Mahony, C. Kelsey, M. Tweedie, F. Perez-Martin, H. McQuaid, D. Diver, D. Mariotti, *Nano Lett.* **2017**, *17*, 1336.
- [16] T. Koh, I. Chiles, M. Gordon, *Appl. Phys. Lett.* **2013**, *103*, 163115.
- [17] L. Liu, A. Corma, *Chem. Rev.* **2018**, *118*, 4981.
- [18] B. H. Kim, M. J. Hackett, J. Park, T. H. Hyeon, *Chem. Mater.* **2014**, *26*, 59.
- [19] W.-H. Chiang, R. M. Sankaran, *Appl. Phys. Lett.* **2007**, *91*, 121503.
- [20] W.-H. Chiang, R. M. Sankaran, *Adv. Mater.* **2008**, *20*, 4857.
- [21] P.-A. Lin, R. M. Sankaran, *Angew. Chem., Int. Ed. Engl.* **2011**, *50*, 10953.
- [22] W.-H. Chiang, M. Sakr, X. P. A. Gao, R. M. Sankaran, *ACS Nano* **2009**, *3*, 4023.
- [23] W.-H. Chiang, R. M. Sankaran, *Nat. Mater.* **2009**, *8*, 882.
- [24] L. L. Lin, S. A. Starostin, V. Hessel, Q. Wang, *Chem. Eng. Sci.* **2017**, *168*, 360.
- [25] L. L. Lin, S. Li, V. Hessel, S. A. Starostin, R. Lavrijssen, W. Zhang, *AIChE J.* **2018**, *5*, 1540.
- [26] A. Ul Haq, S. Askari, A. McLister, S. Rawlinson, J. Davis, S. Chakrabarti, V. Svrcek, P. Maguire, P. Papakonstantinou, D. Mariotti, *Nat. Commun.* **2019**, *10*, 817.
- [27] A. M. Michaels, M. Nirmal, L. E. Brus, *J. Am. Chem. Soc.* **1999**, *121*, 9932.
- [28] Y. C. Cao, R. Jin, C. A. Mirkin, *Science* **2002**, *297*, 1536.
- [29] S. G. Romanov, A. V. Korovin, A. Regensburger, U. Peschel, *Adv. Mater.* **2011**, *23*, 2515.
- [30] Y. Shimizu, K. Kawaguchi, T. Sasaki, N. Koshizaki, *Appl. Phys. Lett.* **2009**, *94*, 191504.
- [31] W.-H. Chiang, C. Richmonds, R. M. Sankaran, *Plasma Sources Sci. Technol.* **2010**, *19*, 034011.
- [32] C. De Vos, J. Baneton, M. Witzke, J. Dille, S. Godet, M. J. Gordon, R. M. Sankaran, F. Reniers, *J. Phys. D: Appl. Phys.* **2017**, *50*, 105206.
- [33] V. S. Santosh, K. Kondeti, U. Gangal, S. Yatom, P. J. Bruggeman, *J. Vac. Sci. Technol., A* **2017**, *35*, 061302.
- [34] N. Khattoon, H. M. Yasin, M. Younus, W. Ahmed, N. U. Rehman, M. Zakaullah, M. Zafar Iqbal, *AIP Adv.* **2018**, *8*, 015130.
- [35] D. Čempel, M. T. Nguyen, Y. Ishida, T. Tokunaga, T. Yonezawa, *New J. Chem.* **2018**, *42*, 5680.
- [36] T. T. Yan, X. X. Zhong, A. E. Rider, Y. Lu, S. A. Furman, K. Ostrikov, *Chem. Commun.* **2014**, *50*, 3144.
- [37] A. Dzimitrowicz, P. Jamroz, M. Nyk, P. Pohl, *Materials* **2016**, *9*, 268.
- [38] D. Sun, J. McLaughlan, L. Zhang, B. G. Falzon, D. Mariotti, P. Maguire, D. Sun, *Langmuir* **2019**, *35*, 4577.
- [39] D. Sun, M. Tang, L. Zhang, B. G. Falzon, D. B. Padmanaban, D. Mariotti, P. Maguire, H. Xu, M. Chen, D. Sun, *Nanotechnology* **2019**, *30*, 455603.
- [40] R.-C. Zhang, D. Sun, R. Zhang, W.-F. Lin, M. Macias-Montero, J. Patel, S. Askari, C. McDonald, D. Mariotti, P. Maguire, *Sci. Rep.* **2017**, *7*, 46682.
- [41] H. Nolan, D. Sun, B. G. Falzon, P. Maguire, D. Mariotti, L. Zhang, D. Sun, *Plasma Processes Polym.* **2019**, *16*, e1800128.
- [42] L. Q. Jing, Y. C. Qu, B. Q. Wang, S. D. Li, B. J. Jiang, L. B. Yang, W. Fu, H. G. Fu, J. Z. Sun, *Sol. Energy Mater. Sol. Cells* **2006**, *90*, 1773.
- [43] J. Zhou, Y. Yang, C. Zhang, *Chem. Rev.* **2015**, *115*, 11669.
- [44] R. M. Sankaran, D. Holunga, R. C. Flagan, K. P. Giapis, *Nano Lett.* **2005**, *5*, 537.
- [45] T. Nozaki, K. Sasaki, T. Ogino, D. Asahi, K. Okazaki, *Nanotechnology* **2007**, *18*, 235603.
- [46] S. Askari, V. Svrcek, P. Maguire, D. Mariotti, *Adv. Mater.* **2015**, *27*, 8011.
- [47] R. K. Gangwar, A. Hamdan, L. Stafford, *J. Appl. Phys.* **2017**, *122*, 243301.
- [48] T. Saito, R. Mitsuya, Y. Ito, T. Higuchi, T. Aita, *Thin Solid Films* **2019**, *669*, 321.
- [49] F. Priolo, T. Gregorkiewicz, M. Galli, T. F. Krauss, *Nat. Nanotechnol.* **2014**, *9*, 19.
- [50] J. Q. Grim, L. Mannaab, I. Moreels, *Chem. Soc. Rev.* **2015**, *44*, 5897.
- [51] X. Ji, F. Peng, Y. Zhong, Y. Su, X. Jiang, C. Song, L. Yang, B. Chu, S.-T. Lee, Y. He, *Adv. Mater.* **2015**, *27*, 1029.
- [52] S. Askari, A. Ul Haq, M. Macias-Montero, I. Levchenko, F. Yu, W. Zhou, K. Ostrikov, P. Maguire, V. Svrcek, D. Mariotti, *Nanoscale* **2016**, *8*, 17141.
- [53] M. Shariat, M. Karimipour, M. Molaei, *Plasma Chem. Plasma Process.* **2017**, *37*, 1133.
- [54] M. Shariat, R. Shaida, M. Karimipour, M. Molaei, *Mater. Res. Express* **2018**, *6*, 015019.
- [55] M. Karimipour, M. Shariat, R. Sheida, M. Molaei, *J. Lumin.* **2019**, *212*, 334.
- [56] C.-C. Yeh, H.-W. Zan, O. Soppera, *Adv. Mater.* **2018**, *30*, 1800923.
- [57] D. Koziej, A. Lauria, M. Niederberger, *Adv. Mater.* **2014**, *26*, 235.
- [58] J. Mei, T. Liao, L. Kou, Z. Sun, *Adv. Mater.* **2017**, *29*, 1700176.
- [59] H. Palneedi, J. H. Park, D. Maurya, M. Peddigari, G.-T. Hwang, V. Annapureddy, J.-W. Kim, J.-J. Choi, B.-D. Hahn, S. Priya, K. J. Lee, J. H. Ryu, *Adv. Mater.* **2018**, *30*, 1705148.
- [60] K. E. Mackie, A. C. Pebley, M. M. Butala, J. P. Zhang, G. D. Stucky, M. J. Gordon, *Appl. Phys. Lett.* **2016**, *109*, 033110.
- [61] T. Koh, E. O'Hara, M. J. Gordon, *J. Cryst. Growth* **2013**, *363*, 69.
- [62] A. C. Pebley, E. Decolvenaere, T. M. Pollock, M. J. Gordon, *Nanoscale* **2017**, *9*, 15070.
- [63] J. Lin, H. Jia, H. Liang, S. Chen, Y. Cai, J. Qi, C. Qu, J. Cao, W. Fei, J. Feng, *Adv. Sci.* **2018**, *5*, 1700687.
- [64] C.-C. Lee, T.-H. Wan, C.-C. Hsu, I.-C. Cheng, J.-Z. Chen, *Appl. Surf. Sci.* **2018**, *436*, 690.
- [65] C. M. Du, M. D. Xiao, *Sci. Rep.* **2014**, *4*, 7339.
- [66] C. S. Ni, D. Carolan, C. Rocks, J. J. Hui, Z. G. Fang, D. B. Padmanaban, J. P. Ni, D. T. Xie, P. Maguire, J. T. S. Irvine, D. Mariotti, *Green Chem.* **2018**, *20*, 2101.
- [67] S. Avivi, Y. Mastai, A. Gedanken, *Chem. Mater.* **2000**, *12*, 1229.
- [68] W. J. Kim, D. Pradhan, Y. Sohn, *J. Mater. Chem. A* **2013**, *1*, 10193.

- [69] S. H. Kim, H. S. Choi, K. D. Jung, *Cryst. Growth Des.* **2016**, *16*, 1387.
- [70] A. L. Costa, M. Serantoni, M. Blosi, E. Mercadelli, L. Esposito, A. Piancastelli, A. Sanson, *Adv. Eng. Mater.* **2010**, *12*, 205.
- [71] J. Wang, Z. Zhang, X. Guo, J. Zhao, H. Chen, X. Yang, *J. Rare Earths* **2010**, *28*, 684.
- [72] X. Li, R. Wang, F. Zhang, D. Zhao, *Nano Lett.* **2014**, *14*, 3634.
- [73] C. Sun, G. Pratz, C. M. Carpenter, H. Liu, Z. Cheng, S. S. Gambhir, L. Xing, *Adv. Mater.* **2011**, *23*, H195.
- [74] Y. Sun, X. Zhu, J. Peng, F. Li, *ACS Nano* **2013**, *7*, 11290.
- [75] L. L. Lin, S. A. Starostin, S. R. Li, S. A. Khan, V. Hessel, *Chem. Eng. Sci.* **2018**, *178*, 157.
- [76] L. L. Lin, X. T. Ma, S. A. Starostin, S. R. Li, V. Hessel, J. Shen, S. M. Shang, H. J. Xu, *ChemistrySelect* **2019**, *14*, 4278.
- [77] L. L. Lin, S. A. Starostin, X. Ma, S. R. Li, S. A. Khan, V. Hessel, *React. Chem. Eng.* **2019**, *4*, 891.
- [78] T. Iqbal, A. Aziz, M. A. Khan, S. Andlee, H. Mahmood, A. A. Khan, R. Khan, M. Shafique, *Mater. Sci. Eng., B* **2018**, *228*, 153.
- [79] T. Iqbal, M. A. Khan, H. Mahmood, *Mater. Lett.* **2018**, *224*, 59.
- [80] Z. D. Mahmoudabadi, E. Eslami, *Electrochim. Acta* **2017**, *245*, 715.
- [81] L. L. Lin, X. Ma, S. Li, M. Wouters, V. Hessel, *Front. Chem. Sci. Eng.* **2019**, *13*, 501.
- [82] T. Velusamy, A. Liguori, M. Macias-Montero, D. B. Padmanaban, D. Carolan, M. Gherardi, V. Colombo, P. Maguire, V. Svrcek, D. Mariotti, *Plasma Processes Polym.* **2017**, *14*, 1600224.
- [83] A. Liguori, T. Galligani, D. B. Padmanaban, R. Laurita, T. V. Gunisha, J. M. Macias-Montero, D. Mariotti, M. Gherardi, *Plasma Chem. Plasma Process.* **2018**, *38*, 1209.
- [84] Z. D. Mahmoudabadi, E. Eslami, *J. Alloys Compd.* **2019**, *793*, 336.
- [85] Z. D. Mahmoudabadi, E. Eslami, M. Narimis, *J. Colloid Interface Sci.* **2018**, *529*, 538.
- [86] R. R. Borude, H. Sugiura, K. Ishikawa, T. Tsutsumi, H. Kondo, N. Ikarashi, M. Hori, *ACS Appl. Nano Mater.* **2019**, *2*, 649.
- [87] R. R. Borude, H. Sugiura, K. Ishikawa, T. Tsutsumi, H. Kondo, M. Hori, *J. Phys. D: Appl. Phys.* **2019**, *52*, 175301.
- [88] X. T. Zheng, A. Ananthanarayanan, K. Q. Luo, P. Chen, *Small* **2015**, *11*, 1620.
- [89] S. Hu, A. Trinchin, P. Atkin, I. Cole, *Angew. Chem., Int. Ed.* **2015**, *54*, 2970.
- [90] V. N. Mochalin, O. Shenderova, D. Ho, Y. Gogotsi, *Nat. Nanotechnol.* **2012**, *7*, 11.
- [91] J. Shen, Y. Zhu, X. Yang, C. Li, *Chem. Commun.* **2012**, *48*, 3686.
- [92] L. Li, G. Wu, G. Yang, J. Peng, J. Zhao, J. J. Zhu, *Nanoscale* **2013**, *5*, 4015.
- [93] X. Zhou, Y. Zhang, C. Wang, X. Wu, Y. Yang, B. Zheng, H. X. Wu, S. W. Guo, J. Y. Y. Zhang, *ACS Nano* **2012**, *6*, 6592.
- [94] Z. Wang, Y. X. Lu, H. Yuan, Z. H. Ren, C. Xu, J. Chen, *Nanoscale* **2015**, *7*, 20743.
- [95] X. Z. Huang, Y. S. Li, X. X. Zhong, A. E. Rider, K. Ostrikov, *Plasma Processes Polym.* **2015**, *12*, 59.
- [96] Q. Y. Wang, Q. Zhang, Y. F. Chen, J. He, K. Jiang, Z. G. Hu, X. X. Zhong, *Plasma Processes Polym.* **2018**, *15*, e1700088.
- [97] J. B. Joffrion, W. Clower, C. G. Wilson, *Nano-Struct. Nano-Objects* **2019**, *19*, 100341.
- [98] X. Ma, S. Li, V. Hessel, L. L. Lin, S. Meskers, F. Gallucci, *Chem. Eng. Process.: Process Intensification* **2019**, *140*, 29.
- [99] J. S. Yang, D. Z. Pai, W. H. Chiang, *Carbon* **2019**, *153*, 315.
- [100] Z. Wang, C. Xu, Y. Lu, G. Wei, G. Ye, T. Sun, J. Chen, *Chem. Eng. J.* **2018**, *344*, 480.
- [101] D. Carolan, C. Rocks, Dilli, B. Padmanaban, P. Maguire, V. Svrcek, D. Mariotti, *Sustainable Energy Fuels* **2017**, *1*, 1611.
- [102] T. Hagino, H. Kondo, K. Ishikawa, H. Kano, M. Sekine, M. Hori, *Appl. Phys. Express* **2012**, *5*, 035101.
- [103] T. Amano, H. Kondo, K. Takeda, K. Ishikawa, M. Hiramatsu, M. Sekine, M. Hori, *Jpn. J. Appl. Phys.* **2018**, *57*, 040303.
- [104] A. Ando, K. Ishikawa, H. Kondo, T. Tsutsumi, K. Takeda, T. Ohta, M. Ito, M. Hiramatsu, M. Sekine, M. Hori, *Jpn. J. Appl. Phys.* **2018**, *57*, 026201.
- [105] H. Uchiyama, K. Ishikawa, Q.-L. Zhao, G. Andocs, N. Nojima, K. Takeda, M. C. Krishna, T. Ishijima, Y. Matsuya, M. Hori, *J. Phys. D: Appl. Phys.* **2018**, *51*, 095202.
- [106] T. Amano, H. Kondo, K. Takeda, K. Ishikawa, M. Hiramatsu, M. Sekine, M. Hori, *Jpn. J. Appl. Phys.* **2018**, *57*, 045101.
- [107] T. Amano, H. Kondo, K. Ishikawa, T. Tsutsumi, K. Takeda, M. Hiramatsu, M. Sekine, M. Hori, *Appl. Phys. Express* **2018**, *11*, 015102.
- [108] N. Bundaleska, J. Henriques, M. Abrashev, A. M. Botelho do Rego, A. M. Ferraria, A. Almeida, F. M. Dias, E. Valcheva, B. Arnaudov, K. K. Upadhyay, M. F. Montemor, E. Tatarova, *Sci. Rep.* **2018**, *8*, 12595.
- [109] A. Kumar, P. A. Lin, A. Xue, B. Y. Hao, Y. K. Yap, R. M. Sankaran, *Nat. Commun.* **2013**, *4*, 2618.
- [110] F. Inzoli, D. Dellasega, V. Russo, R. Caniello, C. Conti, F. Ghezzi, M. Passoni, *Diamond Relat. Mater.* **2017**, *74*, 212.
- [111] S. Iqbal, M. S. Rafique, M. Zahid, S. Bashir, M. A. Ahmad, R. Ahmad, *Mater. Sci. Semicond. Process.* **2018**, *74*, 31.
- [112] C.-H. Nee, M. C. Lee, H. S. Poh, S.-L. Yap, T.-Y. Tou, S.-S. Yap, *Composites, Part B* **2019**, *162*, 162.
- [113] Z. S. Yang, T. Kikuchi, Y. Hatou, T. Kobayashi, H. Shirai, *Jpn. J. Appl. Phys.* **2005**, *44*, 4122.
- [114] R. H. Baughman, A. A. Zakhidov, W. A. De Heer, *Science* **2002**, *297*, 787.
- [115] Q. Cao, J. A. Rogers, *Adv. Mater.* **2009**, *21*, 29.
- [116] L. L. Lin, S. A. Starostin, Q. Wang, V. Hessel, *Chem. Eng. J.* **2017**, *321*, 447.
- [117] K. S. Schramke, Y. Qin, J. T. Held, K. A. Mkhoyan, U. R. Kortshagen, *ACS Appl. Nano Mater.* **2018**, *1*, 2869.
- [118] L. Li, G.-H. Ni, Y.-J. Zhao, Q.-J. Guo, Q.-F. Lin, S.-Y. Sui, H.-B. Xie, W.-X. Duan, *Ceram. Int.* **2018**, *44*, 21810.
- [119] K.-Y. Huang, H.-Y. Chi, P.-K. Kao, F.-H. Huang, Q.-M. Jian, I.-C. Cheng, W.-Y. Lee, C.-C. Hsu, D.-Y. Kang, *ACS Appl. Mater. Interfaces* **2018**, *10*, 900.
- [120] A. Dey, S. Krishnamurthy, J. Bowen, D. Nordlund, M. Meyyappan, R. P. Gandhiraman, *ACS Nano* **2018**, *12*, 5473.
- [121] L. Liu, D. Ye, Y. Yu, L. Liu, Y. Wu, *Carbon* **2017**, *111*, 121.
- [122] T. Ohta, H. Ito, K. Ishikawa, H. Kondo, M. Hiramatsu, M. Hori, C.-J. *Carbon Res.* **2019**, *5*, 40.
- [123] R. R. Borude, H. Sugiura, K. Ishikawa, T. Tsutsumi, H. Kondo, J. G. Han, M. Hori, *Jpn. J. Appl. Phys.* **2019**, *58*, SAAC07.
- [124] A. Demaude, C. Poleunis, E. Goormaghtigh, P. Viville, R. Lazzaroni, A. Delcorte, M. Gordon, F. Reniers, *Langmuir* **2019**, *35*, 9677.
- [125] E. Rogez, B. Claude-Montigny, D. Violleau, J.-P. Rusiecki, O. Motret, *J. Appl. Phys.* **2019**, *125*, 213301.
- [126] Z. Wang, C. Xu, Y. Lu, G. Wei, G. Ye, T. Sun, J. Chen, *Polym. Chem.* **2017**, *8*, 4388.
- [127] S. Ghosh, E. Klek, C. A. Zorman, R. M. Sankaran, *ACS Macro Lett.* **2017**, *6*, 194.
- [128] T. Wang, X. Wang, B. Yang, X. Chen, J. Liu, *J. Electrochem. Soc.* **2017**, *164*, D282.
- [129] R. M. Sankaran, K. P. Giapis, *Appl. Phys. Lett.* **2001**, *79*, 593.
- [130] H. Paetzelt, G. Bohm, Th. Arnold, *Plasma Sources Sci. Technol.* **2015**, *24*, 025002.
- [131] S. A. Al-Bataineh, E. J. Szili, P. J. Gruner, C. Priest, H. J. Griesser, N. H. Voelcker, R. D. Short, D. A. Steele, *Plasma Processes Polym.* **2012**, *9*, 638.
- [132] S. A. Al-Bataineh, R. D. Short, *Plasma Processes Polym.* **2014**, *11*, 263.

- [133] T. S. Anderson, J. H. Ma, S.-J. Park, J. G. Eden, *IEEE Trans. Plasma Sci.* **2008**, *36*, 1250.
- [134] D.-S. Lee, S. Hamaguchi, O. Sakai, S.-J. Park, J. G. Eden, *J. Phys. D: Appl. Phys.* **2012**, *45*, 222001.
- [135] J. Wengler, S. Ognier, M. Zhang, E. Levernier, C. Guyon, C. Ollivier, L. Fensterbank, M. Tatoulian, *React. Chem. Eng.* **2018**, *3*, 930.
- [136] M.-H. Kim, J. H. Cho, S.-J. Park, J. G. Eden, *Eur. Phys. J.: Spec. Top.* **2017**, *226*, 2923.
- [137] M.-H. Kim, J. H. Cho, S. B. Ban, R. Y. Choi, E. J. Kwon, S.-J. Park, J. G. Eden, *J. Phys. D: Appl. Phys.* **2013**, *46*, 305201.
- [138] S.-J. Park, C. M. Herring, A. E. Mironov, J. H. Cho, J. G. Eden, *APL Photonics* **2017**, *2*, 041302.
- [139] J. G. Eden, D. J. Sievers, A. E. Mironov, J. H. Kim, *PCT/US2019/46367*, **2019**.
- [140] a) M. Raeiszadeh, F. Taghipour, *Water Res.* **2019**, *164*, 114959; b) M. Buonanno, B. Ponnaiya, D. Welch, M. Stanislauskas, G. Randers-Pehrson, L. Smilenov, F. D. Lowy, D. M. Owens, D. J. Brenner, *Radiat. Res.* **2017**, *187*, 493.
- [141] H. J. Yang, S.-J. Park, J. G. Eden, *J. Phys. D: Appl. Phys.* **2017**, *50*, 43LT05.
- [142] P. P. Sun, R. Zhang, W. Chen, P. V. Braun, J. G. Eden, *Appl. Phys. Rev.* **2019**, *6*, 041406.
- [143] K. Ostrikov, E. C. Neyts, M. Meyyappan, *Adv. Phys.* **2013**, *62*, 113.
- [144] H. P. Li, K. Ostrikov, W. T. Sun, *Phys. Rep.* **2018**, *770*, 1.
- [145] a) G. V. Naidis, N. Yu. Babaeva, *Phys. Plasmas* **2019**, *26*, 094501; b) A. M. Lietz, M. J. Kushner, *Plasma Sources Sci. Technol.* **2018**, *27*, 105020; c) W. Wang, B. Patil, S. Heijkers, V. Hessel, A. Bogaerts, *ChemSusChem* **2017**, *10*, 2145.
- [146] M. Bonitz, A. Filinov, J.-W. Abraham, K. Balzer, H. Kählert, E. Pehlke, F. X. Bronold, M. Pamperin, M. Becker, D. Loffhagen, *Front. Chem. Sci. Eng.* **2019**, *13*, 201.
- [147] P.-C. Chen, M. Liu, J. S. Du, B. Meckes, S. Wang, H. Lin, V. P. Dravid, C. Wolverton, C. A. Mirkin, *Science* **2019**, *363*, 959.
- [148] K. Ding, D. A. Cullen, L. Zhang, Z. Cao, A. D. Roy, I. N. Ivanov, D. Gao, *Science* **2018**, *362*, 560.
- [149] H. Hartl, J. MacLeod, A. P. O'Mullane, N. Motta, K. Ostrikov, *Small*, <https://doi.org/10.1002/sml.201903184>.
- [150] P. R. Christensen, A. M. Scheuerman, K. E. Loeffler, B. A. Helms, *Nat. Chem.* **2019**, *11*, 442.
- [151] R. Snoeckx, A. Bogaerts, *Chem. Soc. Rev.* **2017**, *46*, 5805.
- [152] R. Hawtof, S. Ghosh, E. Guarr, C. Xu, R. M. Sankaran, J. N. Renner, *Sci. Adv.* **2019**, *5*, eaat5778.